Exploring Black Hole Dynamics

Exploring Black Hole Dynamics

A dissertation presented
by

Hyeyoun Chung

to
The Department of Physics
in partial fulfillment of the requirements
for the degree of
Doctor of Philosophy
in the subject of

Physics

Harvard University
Cambridge, Massachusetts
October 2014

Dissertation advisor

Lisa Randall

Author

Hyeyoun Chung

Exploring Black Hole Dynamics

Abstract

This thesis explores the evolution of different types of black holes, and the ways in which black hole dynamics can be used to answer questions about other physical systems.

We first investigate the differences in observable gravitational effects between a four-dimensional Randall-Sundrum (RS) braneworld universe compared to a universe without the extra dimension, by considering a black hole solution to the braneworld model that is localized on the brane. When the brane has a negative cosmological constant, then for a certain range of parameters for the black hole, the intersection of the black hole with the brane approximates a Banados-Teitelboim-Zanelli (BTZ) black hole on the brane with corrections that fall off exponentially outside the horizon. We compute the quasinormal modes of the braneworld black hole, and compare them to the known quasinormal modes of the three-dimensional BTZ black hole. We find that there are two distinct regions for the braneworld black hole solutions that are reflected in the dependence of the quasinormal modes on the black hole mass. The imaginary parts ω_I of the quasinormal modes display phenomenological similarities to the quasinormal modes of the three-dimensional BTZ black hole, indicating that nonlinear gravitational effects may not be enough to distinguish between a lower-dimensional theory and a theory derived from a higher-dimensional braneworld.

Secondly, we consider the evolution of non-extremal black holes in $\mathcal{N} = 2, d = 4$

supergravity, and investigate how such black holes might evolve over time if perturbed away from extremality. We study this problem in the probe limit by finding tunneling amplitudes for a Dirac field in a single-centered background, which gives the decay rates for the emission of charged probe black holes from the central black hole. We find that there is no minimum to the potential for the probe particles at a finite distance from the central black hole, so any probes that are emitted escape to infinity. If the central black hole is BPS in the extremal limit, then the potential is flat and so there is no barrier to the emission of probes. If the central black hole is non-BPS in the extremal limit, then there is a barrier to emission and we compute the decay rate, which depends both on the charge of the central black hole and the charges of the emitted black holes.

Finally, we consider the possibility that an extremal black hole, the end-point of the evolution of a non-extremal black hole through evaporation, may itself split into a multi-centered black hole solution through quantum tunneling, via a gravitational instanton analogous to the instanton for the symmetric double well in elementary quantum mechanics. We find a gravitational instanton that connects two vacuum states: one state corresponding to a single-centered extremal Reissner-Nordstrom (ERN) black hole configuration, and another state corresponding to a multi-centered ERN configuration. We evaluate the Euclidean action for this instanton and find that the amplitude for the tunneling process is equal to half the difference in entropy between the initial and final configurations.

Contents

List of Figures

List of Tables

Citations to Previously Published Work

Most of Chapter 2 will appear in the following paper:

> "Quasinormal modes of braneworld black holes", H. Chung, L. Randall, M. J. Rodriguez, and O. Varela, *(to appear)*

Most of Chapter 3 has appeared in the following paper:

> "Instability of near-extremal black holes in $\mathcal{N} = 2, d = 4$ supergravity", H. Chung, JHEP 1211:160 (2012), arXiv:1112.4683 [hep-th];

Most of Chapter 4 has appeared in the following paper:

> "Tunneling between single and multi-centered black hole configurations", H. Chung, Phys. Rev. D86, 064036 (2012), arXiv:1201.3028 [gr-qc];

Electronic preprints (shown in `typewriter font`) are available on the Internet at the following URL:

> `http://arXiv.org`

For my mother and father.

Chapter 1

Introduction

Ever since black holes were first discovered as solutions to Einstein's equations of motion, they have been the subject of intense study [1–6]. They are of immense interest in their own right, as the evolution and dynamics of black holes provides a way to investigate strong, nonlinear gravitational effects, and constitutes an environment in which both quantum mechanical and gravitational effects play a significant role, allowing us to probe the ways in which the two theories intersect. Well-posed questions about phenomena in black hole physics have led to fundamental new discoveries by uncovering scenarios that could not be adequately described or explained using existing theories, and pointing us towards newer, sharper descriptions of the physical universe. Probably the most famous example of such a case is the Black Hole Information Paradox [7, 8]. More recently, the Firewall Problem has stimulated a great deal of activity and research in the field by provoking controversy in a similar manner [9–11].

Moreover, black holes have also proven to be of great use as tools for shedding

light on the properties and peculiarities of other physical systems that at first sight appear completely unrelated. The most common such application is through the use of holography and the AdS/CFT correspondence [12–15], which allows a classical black hole solution in AdS space to be interpreted as the dual of a strongly coupled conformal field theory (CFT) at finite temperature, that lives on the boundary of AdS space. The quasinormal modes of a black hole [16–18], which are its characteristic modes of vibration, provide information about the dual CFT, as the mode frequencies have been shown to be dual to the poles of the CFT Green's functions [19–21]. This notion of holography has been extended far beyond the original AdS-Schwarzschild black hole, to encompass conjectured dualities for a wide class of black holes and corresponding quantum systems–in particular, those systems that have thus far stubbornly resisted analytical attack [22, 23]. These dualities give us hope that questions to which we already know the answers in the realm of black hole physics (or questions whose answers are easily computable when framed in relation to black holes) may lead to answers to far more difficult questions in other theories.

1.1 Braneworld Black Holes

The Randall-Sundrum (RS) braneworld models were originally introduced as a potential solution to the hierarchy problem [70, 71]. They consist of a five-dimensional AdS spacetime with either one or two Minkowski branes embedded within it (the former is the RSII model, and the latter is RSI) [24, 25]. These models differ from the Kaluza-Klein models of theories with extra dimensions [26, 27], as the single extra dimension is warped, and in the RSII case, is not compact. The standard model matter fields live

on the four-dimensional brane, and gravity propagates along the extra fifth dimension, though it is localized near the brane due to the curvature of AdS space. Since its original discovery, the applicability of the RS model to theoretical physics has expanded far beyond its original phenomenological roots: in addition to providing a testing ground for any fundamental theory with extra dimensions in which gravity can propagate in the extra dimensions [28, 29], the RS model provides an extension of the AdS/CFT conjecture, referred to as the bulk-brane correspondence [30, 31], where the AdS space is cut off at a small finite distance from spatial infinity in AdS. In this slightly modified scenario, classical gravity in the bulk is conjectured to be dual to a strongly coupled CFT on the brane that is coupled to gravity.

The linear effects of gravity in RS models have been well studied, and it is known that they reproduce four-dimensional Einstein gravity on the brane up to the AdS scale [32–34]. However, the effects of nonlinear gravity in these models are still not well understood. Investigating such effects is crucial in order to find potential phenomenological differences that could tell us whether or not we are living in a braneworld universe; or, at the very least, distinguish between a braneworld scenario and a case in which there is no extra dimension other than the four dimensions on the brane.

Black hole solutions to the RS models provide an ideal setup for exploring such questions, as they necessitate the involvement of nonlinear gravitational effects. Several years ago it was hypothesized that classical black hole solutions that are localized on the brane (rather than existing in the bulk) *cannot exist* in RSII models [35, 36]. This conjecture was supported by evoking the bulk-brane correspondence: the authors pointed out that a large, localized braneworld black hole would be dual to a four-dimensional

black hole in the presence of a strongly coupled CFT. Their calculations indicated that the black hole would Hawking radiate at a high enough rate that the corresponding classical solution in the bulk could not be static. This result, if true, would provide an immediately observable difference between a four-dimensional theory and a five-dimensional one, namely the fact that large, static Schwarzschild black holes could not exist for an observer on the brane in the five-dimensional theory. However, it was later demonstrated that the existence of a static, localized braneworld black hole solution is *not* ruled out by this argument, as the conjecture relied on extrapolating weak coupling calculations for the CFT to the strong coupling case, an assumption that is not necessarily justified [38]. Recently, two groups found numerical solutions for braneworld black hole solutions to RSII using independent methods, providing strong evidence for the existence of such solutions, although it is not yet known whether these solutions are dynamically stable [39, 40]. If the solutions are unstable, then it is still possible that the classical dynamical instability in the bulk could correspond to phenomenological effects on the brane that would distinguish the five-dimensional braneworld black hole from its four-dimensional counterpart in a four-dimensional universe with no extra dimension.

Although the discovery of these black hole solutions is, in and of itself, an enormously significant result, the fact that the solutions are only known numerically means that options for phenomenological investigation are somewhat limited. There are more possibilities in the case of four-dimensional braneworld scenarios, where analytical solutions have been found for localized braneworld black holes, both with zero and non-zero cosmological constant on the brane [41, 42]. It is well known that in three-dimensional gravity with zero cosmological constant, black holes do not exist [43]; ergo, we cannot

compare the braneworld black hole in this case to a corresponding three-dimensional solution. There is, however, a well-known black hole solution in the case of three-dimensional gravity with negative cosmological constant–the Bernado-Teitelboim-Zanelli (BTZ) black hole [44], which is parametrized by the three-dimensional AdS scale L, and the mass of the black hole, M. The localized braneworld black hole solution in the four-dimensional braneworld with a negative cosmological constant on the brane, is parametrized by the four-dimensional AdS scale A, a parameter μ related to the mass of the black hole, and the brane cosmological constant λ; for a certain range of these parameters, the corresponding black hole solution on the brane is a BTZ black hole solution with exponentially decreasing corrections outside the black hole horizon (in this work we will refer to these solutions as BTZ braneworld black holes.) Thus, we can compare the phenomenological characteristics of the braneworld black hole solution to the three-dimensional BTZ solution and ask ourselves if there is any way of distinguishing between the two cases.

One route by which we can institute a comparison between the black holes is to consider the quasinormal modes of both solutions [16–18]. Black hole quasinormal modes are characteristic modes of vibration for the black hole. As the black hole has an event horizon, the boundary value problem for fields on this background is non-Hermitian and thus asymmetric in time. As a result, the system is dissipative, so the characteristic frequencies (the quasinormal mode frequencies) have an imaginary part.

1.2 Evolution of Near-Extremal Black Holes in $\mathcal{N} = 2$, $d = 4$ Supergravity

Multi-centered black hole solutions have been the subject of intense study in their own right for many years [56–60]. More recently, with the discovery of stationary and stable multi-centered solutions in four dimensions, which were free of the string-like singularities and time-dependence of previously known solutions [61, 62], this field of black hole physics has exploded in activity due to the recognition of the importance of these black holes in answering fundamental questions about physics [77, 82]. The well-known supersymmetric multi-centered solutions to supergravity are stablized by balanced electrostatic, gravitational, and scalar forces between the black holes, which allows the black holes to form bound states that are reminiscent of molecules [23, 79, 85].

In addition to having value in providing us with non-trivial solutions to supergravity, these multi-centered configurations have turned out to exhibit many interesting properties that have applications in pure mathematics, as well as the Black Hole Information Paradox [63–66, 77]. The next natural step is to try and identify non-extremal multi-centered solutions, which are expected to share many of the fascinating properties of the extremal solutions, while hopefully allowing us to extend the applicability of those properties [78, 80]. Intuitively, such solutions should exist, as perturbing an existing supersymmetric solution slightly away from extremality by throwing neutral particles into the black holes, should still give a valid solution to the theory. A natural starting point for investigating the possible existence and properties of such solutions is to study the probe limit, in which a multi-centered solution is approximated by point-like probes in the

presence of a central non-extremal black hole. When the supersymmetric multi-centered solution was first discovered, the probe limit was of great value in determining that the potential for a 0-brane probe outside a central extremal black hole, had a stable minimum where the probe could form a stable bound state with the central black hole [66, 82, 85]. A two-centered extremal solution is then formed by fully backreacting this probe solution. Moreover, the distance between the two black holes in this configuration is accurately given by the probe limit. Thus, we expect that the probe limit could also lead us in the right direction in identifying possible bound states that, when fully backreacted, would give a non-extremal multi-centered solution.

In particular, we would like to consider the possibility that an existing, single-centered non-extremal solution could evolve by the emission of smaller, "satellite" black holes to form a multi-centered solution. If the emission of such black holes can occur with a finite probability, then either they will escape to infinity, or to the minimum of a potential at some finite distance from the parent black hole, forming a stable bound state, and thus admitting the possibility that a single-centered non-extremal black hole solution might evolve to a multi-centered solution over time. Numerical work has been done on the probe potentials for BPS probes around a central BPS black hole in $\mathcal{N} = 2, d = 4$ supergravity that shows that for certain parameters of the black hole charges, stable minima do indeed exist that could allow for the formation of non-extremal multi-centered configurations [79]. For other regions of the phase space, stable minima do not exist and the central non-extremal black hole merely evolves by emitting BPS probe particles to infinity. As the numerical investigations consisted of computing the minima of the probe potential and identifying whether or not the formation of a bound state was possible, decay rates have

not yet been computed for these processes.

In addition to being a problem of great inherent interest in either leading us to possibly identify a new class of non-extremal black hole solutions, or giving us new information about the semiclassical evolution of non-extremal black holes, this question has the potential to shed light on the evolution of complex condensed matter systems that have been conjectured to be dual to the multi-centered black hole solutions of supergravity. These conjectured duals essentially consist of "glassy" systems, such as spin glasses [67] and electron glasses [68], which are characterized by vacuum landscapes with exponentially many minima. Although this conjecture is still in its early stages, the immense difficulty of directly analyzing glass-like systems prompts us to pursue the hypothetical duality in the hopes that existing knowledge about black holes may shed light on other phenomena that remain stubbornly mysterious. There are striking similarities that support the interpretation of multi-centered black hole solutions as holographic duals of glasses. When these black hole solutions exist, there are exponentially many stable configurations (as the only parameters that need to remain constant are the total mass and charge, which may be distributed in many different ways among multiple black holes.) Heating the multi-centered black hole configuration is equivalent to moving the black holes away from extremality, which can be accomplished by adding more and more neutral particles to the black holes. Eventually this will cause the multiple black holes to collapse into a single black hole under the attractive force of gravity, which is analogous to the behavior of glasses in melting into a liquid upon being heated. However, like a glass that slowly cools and may become stuck in local vacua (rather than the single vacuum that globally minimizes the free energy) while doing so, a non-extremal single-centered black hole, or a non-extremal configuration, will

only slowly evolve to extremality or to form a multi-centered extremal configuration, due to the suppression of the emission of particles from a black hole that is necessary to move charges from one center to another, in order to evolve to a state with lower free energy.

1.3 Tunneling between single and multi-centered black hole configurations

The evolution of a non-extremal black hole, as described in Section 1.2, will eventually cause it to become extremal. There are many unanswered questions about the precise nature of the endpoint of this evolution [94]. In particular, we know of the existence of multiple multi-centered extremal black hole configurations with the same total mass and charge. All of these configurations are stable, and thus correspond to different vacuum states. Is it possible for quantum tunneling to take place between these different vacua, so that the final state after the evaporation of a non-extremal black hole is in fact a superposition over all possible multi-centered extremal black holes? Is it possible for a single-centered extremal black hole to split into a multi-centered solution?

The geometry of $AdS_2 \times S_2$ is crucial for investigating this problem, as it forms the near-horizon geometry of all known supersymmetric black holes with non-zero entropy. The simplest case is the Reissner-Nordstrom black hole [69], but there are far more complicated examples in string theory that have multiple charges and additional fields [85]. If we allow for topological changes in spacetime through quantum tunneling, then a tunneling process between different geometries can be described by a gravitational instanton [73, 98]. Instantons are solutions to the Euclidean equations of motion, and can be classified

into two categories: instantons representing decay processes through quantum tunneling, and instantons representing mixing between degenerate vacua. In the case of elementary quantum mechanics, the first category is typified by tunneling through a potential barrier, and the second category is typified by the mixing of degenerate localized states in a one-dimensional symmetric double well, so that the ground state is a superposition of these two states. In the first case, the instanton can be connected to a Lorentzian solution to the equations of motion by splitting the instanton solution in half across a time-symmetric surface. In the second case, the instanton should be able to connect to Lorentzian solutions across both an initial constant-time hypersurface and a final constant-time hypersurface.

Gravitational instantons have been identified for processes such as the pair production of charged black holes in a vacuum, in an analogy to Schwinger pair production in the presence of an electric field [91]. They have also been used to describe the fragmentation of AdS space: an instanton in the probe limit describes the fragmentation of an $AdS_2 \times S_2$ space with charge $Q_1 + Q_2$ into an $AdS_2 \times S_2$ space with charge Q_1 and a probe 0-brane of charge Q_2 being emitted to the spatial infinity of the first $AdS_2 \times S_2$ space [93]. Moving away from the probe limit, the Brill Instanton is a gravitational instanton that describes the fragmentation of a single $AdS_2 \times S_2$ universe into several separate, disconnected $AdS_2 \times S_2$ universes, with the same total charge [92].

In order to consider the possibility of quantum mixing between charged black hole configurations with different numbers of charged centers, we would like to consider a tunneling process that connects a single-centered $AdS_2 \times S_2$ geometry to a multi-centered $AdS_2 \times S_2$ geometry of the same total charge, but where the multiple throats remain joined at the "top" in a single $AdS_2 \times S_2$ universe, rather than disconnecting completely from each

other as in the case of the Brill instanton. Such an instanton represents mixing between a single-centered black hole configuration and a configuration where the single center has split into multiple centers at the bottom of the black hole throat. It is then possible that these multiple centers could tunnel out of the black hole throat and escape the horizon of the original black hole center, in order to form a multi-centered solution where the throats are entirely separated from each other in space.

1.4 Outline of the Thesis

In this thesis we study three problems that investigate the evolution of black holes, whose dynamics are closely tied to the properties of other physical systems. The first problem, described in Chapter 2, investigates the phenomenology of black holes in different cosmological models. The second problem, described in Chapter 3, studies the evolution of non-extremal black holes in $\mathcal{N} = 2$ SUGRA. The third and final problem, described in Chapter 4, is to calculate quantum tunneling rates between single and multi-centered black hole configurations. Here we briefly outline the results covered in each chapter.

In Chapter 2, we address the question of finding the quasinormal modes for a conformal scalar field in the background of a localized braneworld black hole in a four-dimensional braneworld. The class of braneworld black hole solutions that we consider have the property that the intersection of the black hole with the brane is the three-dimensional BTZ black hole, up to exponentially suppressed corrections. We compute the conformal scalar field quasinormal modes of the braneworld black hole, and find that there are two

distinct regions for the system, reflected in the dependence of the quasinormal modes on the black hole mass. We also compare the quasinormal modes to the quasinormal modes of a conformal scalar field in the background of an ordinary three-dimensional BTZ black hole, and find that there are phenomenological similarities between the two theories, thus indicating that the non-linear gravitational dynamics of a lower-dimensional theory may be reproduced on the brane by the braneworld setup.

In Chapter 3, we consider the evolution of non-extremal black holes in $\mathcal{N} = 2, d = 4$ supergravity, and investigate how such black holes might evolve over time if perturbed away from extremality. We study this problem in the probe limit by finding tunneling amplitudes for a Dirac field in a single-centered background, which gives the decay rates for the emission of charged probe black holes from the central black hole. We find that there is no minimum to the potential for the probe particles at a finite distance from the central black hole, so any probes that are emitted escape to infinity. If the central black hole is BPS in the extremal limit, then the potential is flat and so there is no barrier to the emission of probes. If the central black hole is non-BPS in the extremal limit, then there is a barrier to emission and we compute the decay rate, which depends both on the charge of the central black hole and the charges of the emitted black holes.

In Chapter 4, we consider the possibility that an extremal black hole, the end-point of the evolution of a non-extremal black hole through evaporation, may itself split into a multi-centered black hole solution through quantum tunneling, via a gravitational instanton analogous to the instanton for the symmetric double well in elementary quantum mechanics. We find a gravitational instanton that connects two vacuum states: one state corresponding to a single-centered extremal Reissner-Nordstrom (ERN) black hole

configuration, and another state corresponding to a multi-centered ERN configuration. We evaluate the Euclidean action for this instanton and find that the amplitude for the tunneling process is equal to half the difference in entropy between the initial and final configurations. This result suggests that after a charged non-extremal black hole becomes extremal through the emission of charged particles, the final result is not a single extremal black hole but rather a quantum superposition of all multi-centered extremal black hole states with the same total mass and charge.

Chapter 2

Quasinormal Modes of BTZ Braneworld Black Holes

In this chapter we study the phenomenology of Banados-Teitelboim-Zanelli (BTZ) black holes in a four-dimensional braneworld model and in the ordinary three-dimensional case. We consider a class of four-dimensional braneworld black hole solutions that give a BTZ black hole on the three-dimensional brane up to corrections that decrease exponentially outside the horizon. We compute the quasinormal mode (QNM) frequencies of a conformal scalar field in this black hole background, and in addition to studying these QNM in their own right, we compare them to the quasinormal mode frequencies of a conformal scalar field on the background of a three-dimensional BTZ black hole. We find that the variation of the quasinormal mode frequencies of the braneworld black holes, with the black hole mass, differs qualitatively for large black holes compared to small black holes, indicating two distinct regions in the bulk theory (and the corresponding dual theory on

the brane.) Furthermore, we find qualitative and quantitative similarities between these quasinormal mode frequencies and the QNM frequencies of the strictly three-dimensional theory.

In Section 2.1.1 we describe the braneworld black hole solutions under investigation. In Section 2.2 we briefly cover the concept of black hole quasinormal modes, and in Section 2.2.1 we outline our strategy for computing the eigenvalues of the radial and angular equations of motion for a conformal scalar field in the background of the braneworld black hole. In Section 2.3 we describe the quasinormal modes of a conformally coupled scalar field in the background of the braneworld black hole. In Section 2.4 we compare these quasinormal modes to the QNM of the three-dimensional BTZ black hole, and we conclude in Section 2.5.

2.1 Introduction

2.1.1 Randall-Sundrum Braneworld Black Holes

The search for black hole solutions in Randall-Sundrum (RS) braneworlds that are localized on the brane rather than existing in the bulk, has proved to be an unexpectedly difficult problem. It is only recently that numerical analysis has yielded what appear to be genuine static localized black hole solutions in the five-dimensional RSII model, though it is not yet known whether these solutions are dynamically stable [39, 40]. In fact, it was conjectured several years ago that such solutions could not exist. The conjecture rested on using the bulk-brane correspondence to predict that the four dimensional black hole would evaporate too rapidly via Hawking radiation to allow the dual classical solution

in the braneworld to be static. Ultimately, all of these investigations address the larger problem of nonlinear gravitational effects in the braneworld picture. It is known that the RS model reproduces four-dimensional gravity on the brane at the linear level: however, we do not know if there are significant nonlinear effects that could easily differentiate between a lower-dimensional universe that ultimately derives from a higher-dimensional braneworld, or a lower-dimensional universe that is not embedded as a brane in a higher-dimensional universe. Black holes provide an ideal framework for asking these questions, as we expect nonlinear gravitational effects to be most easily accessible through studying black holes. Unfortunately, the lack of analytical solutions for localized braneworld black holes in the five-dimensional RSII model makes it difficult to pinpoint illuminating calculations.

There are, however, known analytical braneworld black hole solutions in AdS_4 that correspond to black holes localized on the 2-brane [41, 42]. When the brane is an asymptotically flat space, there is no corresponding classical solution for a three-dimensional black hole in asymptotically flat space *without* a braneworld. The corresponding three-dimensional black hole is conjectured to be the quantum backreacted solution for a point mass (of a strongly coupled conformal field theory) [36]. When the brane has a negative cosmological constant, however, the corresponding classical solution is the BTZ black hole. That is, there is a braneworld black hole or black string solution in AdS_4 such that the solution on the brane is either the BTZ black hole, or the BTZ black hole plus corrections that fall of exponentially outside the black hole horizon. The existence of these solutions allows for the comparison of quasinormal modes of the braneworld black holes, with quasinormal modes of the BTZ black hole. Any phenomenological differences could provide intersesting insights into the bulk-brane correspondence, as well as a possible route

to distinguishing braneworld physics from lower-dimensional physics in a non-braneworld scenario.

2.1.2 Exact braneworld black hole solutions

The known analytical black hole solutions in a four-dimensional AdS_4 braneworld are constructed by starting with the following solution to Einstein's equations with negative cosmological constant describing accelerating black holes in AdS_4:

$$ds^2 = \frac{1}{A^2(x-y)^2}\left(H(y)dt^2 - \frac{dy^2}{H(y)} + \frac{dx^2}{G(x)} + G(x)d\phi^2\right) \tag{2.1}$$

where

$$H(y) = -\lambda + ky^2 - 2\mu A y^3 \tag{2.2}$$

$$G(x) = 1 + kx^2 - 2\mu A x^3 \tag{2.3}$$

and $k = 1, 0, -1$. The case of $\lambda = 0$ and $k = -1$ gives braneworld black holes with asymptotically flat branes. In this work, however, we consider $\lambda > 0$ and $k = +1$, which gives a spacetime that can be used to construct braneworld black holes with negative cosmological constant on the brane. In order to see how the above geometry is related to AdS_4, we define the coordinates

$$\hat{r} = \frac{\sqrt{y^2 + \lambda x^2}}{A(x-y)} \tag{2.4}$$

$$\hat{\rho} = \sqrt{\frac{1+x^2}{y+\lambda x^2}} \tag{2.5}$$

Under this change of coordinates, the metric (2.1) becomes

$$ds^2 = \frac{d\hat{r}^2}{\frac{\hat{r}^2}{A^2(\lambda+1)} - \lambda} + \hat{r}^2\left(-(\lambda\hat{\rho}^2 - 1)dt^2 + \frac{d\hat{\rho}^2}{\lambda\hat{\rho}^2 - 1} + \hat{\rho}^2 d\phi^2\right), \tag{2.6}$$

which can be shown to be a parametrization of AdS_4 [45].

We construct the braneworld solutions from the above spacetime as in the case of asymptotically flat branes, by cutting the spacetime along two hypersurfaces, and gluing it to a copy of itself along both hypersurfaces. It is necessary to cut the spacetime along two surfaces rather than one, in order to avoid singularities. Thus we end up with a spacetime with two branes. It turns out that both branes have positive tension. The two hypersurfaces chosen for cutting and gluing are those defined by $x = 0$, $y = 0$, and correspond to slices of constant $\hat{r}$ where the coordinate $\hat{r}$ is defined by

$$\hat{r} = \frac{\sqrt{y^2 + \lambda x^2}}{A(x - y)} \tag{2.7}$$

and corresponds to a coordinate foliating the AdS_4 space. When the parameter $\mu > 0$, the function $G(x)$ has a single positive root at $x = x_2$. Then the periodicity of the coordinate ϕ is chosen to be

$$\Delta\phi \equiv 2\pi\beta \equiv \frac{4\pi}{|G'(x_2)|} \tag{2.8}$$

in order to avoid a conical singularity at $x = x_2$. In the case of $\mu = 0$, the periodicity of ϕ may be chosen arbitrarily to be any $\Delta\phi$, as there is no conical singularity at $x = x_2$.

Large black holes on the brane, which corresponds to the above solution with $\mu = 0$, agree exactly with the BTZ black hole, which has the metric

$$ds^2 = (r^2/L^2 - M)d\hat{t}^2 - (r^2/L^2 - M)^{-1}dr^2 - r^2 d\hat{\phi}^2 \tag{2.9}$$

where M is the mass of the BTZ black hole and the horizon radius is given by

$$r_h = \frac{M^{1/2}}{L}. \tag{2.10}$$

However, in the bulk the four-dimensional solution forms a BTZ black string rather than a localized black hole. For smaller mass black holes on the brane, there are two different classes of black hole solutions; in both cases, the black hole on the brane is the BTZ black hole with corrections that are negligible outside the horizon for the solution with smaller area. The geometry on the 2-brane is (introducing new coordinates ρ):

$$ds^2 = \frac{1}{A^2}\left[-\left(\lambda\rho^2 - k - \frac{2\mu A}{\rho}\right)dt^2 + \left(\lambda\rho^2 - k - \frac{2\mu A}{\rho}\right)^{-1} d\rho^2 + \rho^2 d\phi^2\right] \tag{2.11}$$

where we have defined

$$\rho = \frac{1}{y} \tag{2.12}$$

When $k = +1$, the above metric is similar to the BTZ metric, but with extra $\mu A/\rho$ corrections. These extra terms are negligible outside the horizon if $2\mu A << \lambda^{-1/2}$. We can write the above metric in the form of the BTZ metric as given in (2.9) by defining the following coordinates in the case $\mu > 0$:

$$r \equiv \frac{\beta}{A}\rho \tag{2.13}$$

$$\hat{t} \equiv \frac{1}{A\beta}t \tag{2.14}$$

$$\hat{\phi} \equiv \frac{1}{\beta}\phi \tag{2.15}$$

This gives the BTZ metric (plus the previously mentioned corrections) with

$$\frac{1}{L^2} \equiv \lambda A^2 \tag{2.16}$$

$$M \equiv \beta^2 \tag{2.17}$$

It can be shown that this value M is both the three-dimensional mass M_3 of the black hole on the brane (obtained by comparing the asymptotic geometry as $\rho \to \infty$ with the

geometry of the BTZ black hole, and the four-dimensional thermodynamic mass M_4 of the braneworld black hole, obtained by integrating $\delta M = T\delta S$ [42]. Thus from now on we will refer to this quantity simply as M without a subscript.

2.2 Black Hole Quasinormal Modes

The quasinormal modes of a black hole form its characteristic modes of vibration, and thus provide an excellent "fingerprint" for the spacetime. Quasinormal modes can be defined for any type of perturbation, whether scalar, Dirac, electromagnetic, or gravitational, and are found by solving for the form of the fields and then imposing boundary conditions at the black horizon and at spatial infinity, which restricts the allowed frequencies to the mode frequencies. A distinctive feature of these modes is that the frequencies have an imaginary part, indicating that they decay exponentially over time–they are thus not normal modes in the usual sense.

The main question that we would like to investigate is comparing the characteristics of the black holes described in Section 2.1.1, which are ultimately derived from a braneworld picture, as opposed to the characteristic of BTZ black holes in a 3-dimensional universe with no braneworld. We do this by comparing the quasinormal modes of the two classes of black holes. Any significant difference in these results could point to a way of distinguishing a 3-dimensional visible universe that derives from a higher-dimensional braneworld picture, as opposed to a lower-dimensional universe that is not derived from a braneworld.

2.2.1 A Conformal Scalar Field in the Braneworld Background

We consider a conformally coupled scalar field Φ, whose equation of motion in four dimensions is

$$\nabla^2\Phi - \frac{1}{6}\mathcal{R}\Phi = 0 \tag{2.18}$$

As the equation of motion is conformally invariant, we can use the metric multiplied by the conformal factor $A^2(x-y)^2$, in order to simplify the equations. We also rescale the coordinates (t, ϕ) as indicated in (2.13), for ease of comparison with the three-dimensional BTZ black hole. Substituting the ansatz:

$$\Phi = e^{i(m\phi-\omega t)}Y(y)S(x) = e^{i(\hat{m}\hat{\phi}-\hat{\omega}\hat{t})}Y(y)S(x) \tag{2.19}$$

for the conformal scalar field, we find that the equations of motion do separate, and we end up with:

$$2x(1-3A\mu x)S'(x) + G(x)S''(x) - \frac{\hat{m}^2}{\beta^2 G(x)}S(x) + KS(x) + 2A\mu x S(x) = 0 \tag{2.20}$$

$$2y(1-3A\mu y)Y'(y) + H(y)Y''(y) - \frac{\hat{\omega}^2}{A^2\beta^2 H(y)}Y(y) + KY(y) - 2A\mu y Y(y) = 0, \tag{2.21}$$

where K is the separation constant.

The Angular Equation

We are only interested in the angular equation for $S(x)$ in order to find its eigenvalues, so that we can insert the appropriate separation constant K into the radial equation. Recall that the coordinate x has range $x \in [0, x_2]$, where x_2 is the single positive root of $G(x)$. Usually in the numerical determination of QNM, the angular equation can be solved

exactly and only the radial part requires numerical methods. However, in this case we need numerical methods for both equations since the angular equation cannot be solved exactly.

Studying the differential equation (2.20) for $S(x)$ shows that it has four regular singular points, three at the three distinct roots of $G(x)$ (one of them being $x = x_2$), and one at $x = \infty$. As all the singular points are regular, we can use Frobenius' method to expand the solution in a power series about each singular point, where each power series has a radius of convergence that reaches at least to the closest regular singular point. Closer investigation shows that x_2 is the only root of $G(x)$ with a positive real part. Thus, by expanding the solution in a power series about $x = x_2$, the radius of convergence of this power series certainly encompasses the point $x = 0$, and the brane boundary condition can be imposed on the series at $x = 0$. This allows us to solve for the separation constant K. The computation is outlined in Section A.1. Note that direct calculation shows that the quasinormal mode frequencies are not particularly sensitive to small changes in the eigenvalue K, so we do not have to obtain the K values to extremely high levels of accuracy in order to find the quasinormal modes–computing to two significant figures is enough. The details of the computation are outlined in Section A.1.

As the polynomial $G(x)$ is fully determined by the parameter μA, fixing μ and A alone is enough to determine K. Using this method to find K for various μ and A gives a list of possible K values for each set of parameters. In order to narrow the field of study, the smallest value of K was taken for each (μ, A), and we let the quantum number $\hat{m}$ take the values $\{0, 1, 2\}$. The mass of the black-hole (the three-dimensional mass M_3 and the four-dimensional mass M_4 are the same for these braneworld black holes) can also be

determined with only (μ, A), as the mass is given by [42]:

$$M_3 = \frac{\beta^2}{8G_3} \tag{2.22}$$

The Radial Equation

Studying the differential equation (2.21) for $Y(y)$ shows that it too has four regular singular points, three at the three distinct roots of the polynomial $H(y)$ (one of them being $y = y_h$), and one at $y = -\infty$. As all the singular points are regular, we can use Frobenius' method again in order to expand $Y(y)$ in a power series about each singular point. The absolute magnitude of the two complex roots of $H(y)$ is always greater than the magnitude of y_h, and thus if we expand the solution $Y(y)$ in a power series about the regular singular point $y = y_h$, the radius of convergence of this power series will always encompass $y = 0$, and we can impose the necessary boundary conditions at $y = y_h$ and $y = 0$ on a single power series. We can therefore use the series method outlined above for $S(x)$ to compute the quasinormal modes $\hat{\omega}$. However, rather than straightforwardly solving the equation (2.21) for $\hat{\omega}$, we make two changes. Firstly, we change the variable $Y(y)$ to make it easier to identify ingoing and outgoing modes at the black hole horizon, and impose ingoing-only boundary conditions there. Defining a new variable $\Psi(y)$ by:

$$\Phi(t, y) = e^{-i\hat{\omega}(\hat{t}+r_*)}\Psi(y), \tag{2.23}$$

where r_* is the tortoise coordinate (defined with a minus sign as y is negative on the entire range from the black hole horizon to spatial infinity, where $y = 0$, so that ρ decreases from the horizon to $\rho \to -\infty$ at spatial infinity):

$$r_* \equiv -\int \frac{d\rho}{\rho^2 H(\rho)} = -\int \frac{dy}{H(y)} \tag{2.24}$$

we see that ingoing modes have $\Psi(y) = O(1)$, and outgoing modes, which have the form $\Phi(t, y) \sim e^{-i\hat{\omega}(\hat{t}-r_*)}$, have $\Psi(y) \sim e^{2i\hat{\omega}r_*}$. Substituting this form for the field into the equation of motion for $Y(y)$ gives:

$$H(y)\partial_y^2\Psi + \left(H'(y) + \frac{2i\hat{\omega}}{A\beta}\right)\partial_y\Psi + (K - 2\mu Ay)\Psi = 0 \tag{2.25}$$

We know that ingoing modes have the form $\Psi(y) = O(1)$. And using the fact that:

$$r_* = -\int \frac{dy}{H(y)} \approx -\frac{1}{H'(y_h)}\ln(y - y_h), \tag{2.26}$$

we find that outgoing modes have the form $\Psi(y) \sim (y - y_h)^{-2i\hat{\omega}/H'(y_h)}$. This information allows us to identify the correct independent solution when expanding $\Psi(y)$ around the point $y = y_h$. We can now proceed to solve numerically for $\hat{\omega}$ in the same way that we solved numerically for K in the previous section. The details of the computation are outlined in Appendix A.2.

Boundary Conditions

It is worth taking a closer look at the boundary conditions we impose both for finding the quasinormal modes of the braneworld black hole and black string. Typically, for scalar fields we impose ingoing boundary conditions at the horizon to compute quasinormal modes, and either outgoing boundary conditions at infinity in asymptotically flat space, or Dirichlet boundary conditions at infinity in AdS space [16, 17]. There is greater freedom in choosing boundary conditions for gravitational and electromagnetic perturbations, and several viable possibilities have been proposed [51, 52].

In our setup, we impose ingoing boundary conditions as the black hole horizon as usual. At spatial infinity (corresponding to $y = 0$), the particular geometry of this

braneworld setup requires us to impose different boundary conditions from the standard ones in this case. Our braneworld scenario has two branes, one at $x = 0$, and another at $y = 0$, with $\mathbb{Z}_2$ symmetry about both branes. The $\mathbb{Z}_2$ symmetry can be relaxed in cases where the brane is thick [54, 55], so that the cosmological constant is different on either sides of the brane, but otherwise, reflection symmetry about the brane should be preserved. It would be nonsensical for the scalar field solution (or any aspects of the solution) to be different after reflection about the brane. Imposing $\mathbb{Z}_2$ symmetry about the brane at $y = 0$ amounts to imposing Neumann boundary conditions at spatial infinity. Another possibility is to eliminate the second brane at $y = 0$. This brane is necessary in order to keep all the bulk modes normalizable. This condition may be satisfied by imposing Dirichlet boundary conditions at $y = 0$ instead. These boundary conditions are also imposed on the quasinormal modes, in which case we get the usual setup of ingoing boundary conditions at the black hole horizon and Dirichlet boundary conditions at spatial infinity.

When comparing these quasinormal modes to the quasinormal modes of the three-dimensional theory with a BTZ black hole background, we should make sure that the boundary conditions are consistent. This is easily imposed at the horizon, as we have ingoing boundary conditions in all cases. When considering the boundary conditions as spatial infinity, it makes a difference whether we are considering a conformally coupled or a minimally coupled scalar field on the BTZ background. We can write the radial equation of motion for this field in the standard form (where ρ is a radial coordinate and r_* is a tortoise coordinate defined in terms of ρ that goes to $-\infty$ at the black hole horizon and ∞

at spatial infinity):

$$\partial_{r_*}^2 R(\rho) + V(\rho)R(\rho) = 0, \tag{2.27}$$

where $V(\rho)$ is a potential that depends on the type of field we are considering. In the case of a conformally coupled scalar field, $V(\rho)$ is finite at spatial infinity, so we can impose either Neumann or Dirichlet boundary conditions so as to be consistent with the boundary conditions imposed in the full four-dimensional braneworld setup. In the case of a minimally coupled scalar field, $V(\rho)$ contains a ρ^2 term that blows up as $r_* \to \infty$, which forces us to impose Dirichlet boundary conditions at spatial infinity. Thus in that case we can only compare the quasinormal mode frequencies to those of the braneworld setup where we have also imposed Dirichlet boundary conditions at $y = 0$.

2.2.2 Numerical Computation of the Angular and Radial Eigenvalues

In order to study the quasinormal modes for black holes that lie outside the limit $\mu A <<< 1$, we carry out a numerical analysis of the eigenvalues of the equations of motion. This can be done by expanding the solutions in power series about the regular singular points on the real line, and then using the equations of motion to define recurrence relations between the coefficients in the power series. In the case of our equations of motion, we must carry out this procedure in order to find the eigenvalues K of the angular equation, as well as the quasinormal frequencies ω given by the radial equation. The computations are outlined in Appendix A.1–A.2.

Table 2.1 *Numerically computed values of the eigenvalue K of the radial equation of motion and the black hole mass M, for various values of the parameters μ, A and angular momentum quantum number $\hat{m} = 0$. The smallest value of K found is given in each case, to three significant figures.*

(μ, A)	K	M_3
(0.2, 0.2)	0.512	0.0243
(0.25, 0.25)	0.408	0.055
(0.4, 0.4)	0.517	0.218
(0.5, 0.5)	0.550	0.303
(0.6, 0.6)	0.609	0.333
(1, 1)	0.968	0.25
(1.5, 1.5)	1.51	0.157
(2, 2)	2.13	0.109
(3, 3)	3.52	0.064
(3.5, 3.5)	4.29	0.064
(5, 5)	6.80	0.0327

Table 2.2 *The imaginary and real parts ω_I and ω_R of the dominant quasinormal mode, and the black hole mass M, for various values of the parameters (μ, A), when $\Lambda = 0.001$. These values were obtained using the Dirichlet boundary condition at $y = 0$, and the smallest value of the eigenvalue K obtained from the angular equation, and angular momentum quantum number $\hat{m} = 1$.*

(μ, A)	M_3	$-\omega_I$	ω_R
(0.2, 0.2)	0.0243	0.0074	0.0091
(0.25, 0.25)	0.055	0.011	0.014
(0.4, 0.4)	0.218	0.022	0.027
(0.5, 0.5)	0.303	0.026	0.031
(0.6, 0.6)	0.333	0.028	0.034
(1, 1)	0.25	0.024	0.039
(2, 2)	0.109	0.013	0.041
(3, 3)	0.064	0.011	0.042
(5, 5)	0.0327	0.009	0.042

2.3 The Quasinormal Modes of the Braneworld Black Hole

In this section we present our results for the computation of the angular eigenvalues K and the quasinormal modes ω for a conformally coupled scalar field in the background of a braneworld black hole. We have found that our results were qualitatively similar for both Dirichlet and Neumann boundary conditions, so in the rest of this work we will only specifically mention results obtained for Dirichlet boundary conditions. As stated above, in computing ω we took the lowest value of K for each set of parameters (λ, μ, A), and carried out our calculations for $\hat{m} \in \{0, 1, 2\}$ (further calculations showed that our results are actually independent of K, which is another respect in which there are phenomenological similarities between the three and four-dimensional theories–the spheroidal eigenvalue K does not affect the quasinormal modes.) As our ultimate aim was to compare the full four-dimensional theory to a three-dimensional theory, we kept the value of the three-dimensional cosmological constant on the brane, $\Lambda \equiv 1/L^2 = \lambda A^2$, constant when varying μ and A. Note that μA parameterizes the size of the four-dimensional braneworld black hole.

Figure 2.1 shows the dependence of the first three values of $K \equiv \nu(\nu + 1)$ on the parameter μA (only the product μA matters in determining K), for values of the quantum number $\hat{m} = \{0, 1, 2\}$. When it comes to the quasinormal modes ω, we find that there are two distinct regions of parameter space depending on the value of μA. The dependence of the real and imaginary parts ω_R and ω_I on μA when μA is less than a particular critical value (approximately 0.36, corresponding to $M \approx 0.33$), is radically different from the dependence of ω_R and ω_I on μA when μA is greater than the critical value. In order to aid

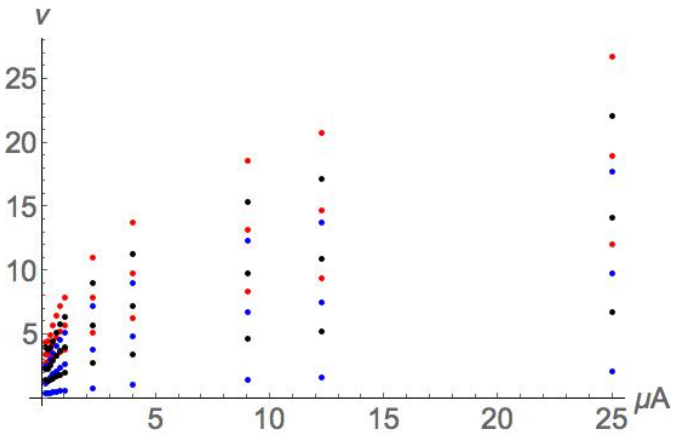

Figure 2.1 *The eigenvalues of the spheroidal equation for various values of the parameter* $\mu A = (0.04, 0.0625, 0.16, 0.25, 0.36, 0.49, 0.64, 0.81, 1, 2.25, 4, 9, 12.25, 25, 64, 100)$. *The red dots have* $\hat{m} = 0$, *the blue dots have* $\hat{m} = 1$, *and the black dots have* $\hat{m} = 2$.

with our aim of comparing the dynamics of the four-dimensional theory to the dynamics of a three-dimensional theory, we plotted ω_R and ω_I against the mass M of the black hole (or quantities depending only on M), as the three-dimensional mass of the black hole on the brane, M_3, is equal to the full thermodynamic four-dimensional mass of the braneworld black hole, M_4, so that we have $M = M_3 = M_4$ as stated in Section 2.1.2.

For the region of small μA, we find that ω_I depends linearly on $\sqrt{M}$, as shown in Figure 2.4. The real part ω_R of the quasinormal modes do not depend linearly on $\sqrt{M}$, but do increase with this quantity, as shown in Figure 2.5. Both ω_R and ω_I approach zero as $M \to 0$. These trends disappear when Λ becomes too large (of order $O(10)$), without a corresponding increase in A so that λ remains small (since $\lambda A^2 = \Lambda$.) This is because

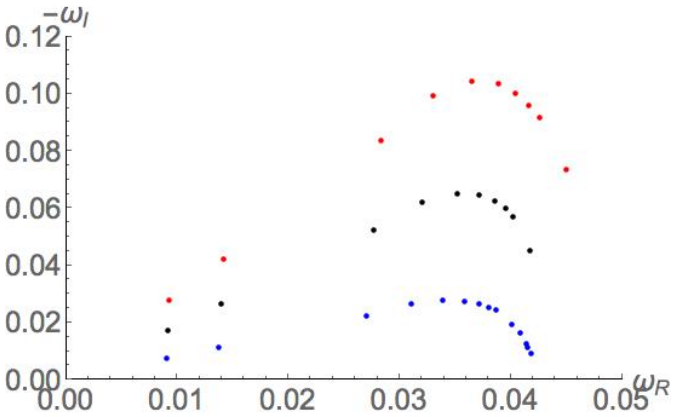

Figure 2.2 *The imaginary and real parts of the quasinormal modes for various values of the parameter* $\mu A = (0.04, 0.0625, 0.16, 0.25, 0.36, 0.49, 0.64, 0.81, 1, 2.25, 4, 9, 12.25, 25)$, *when* $\Lambda = 0.001$ *and* $\hat{m} = 1$. *The blue dots are the first overtone* $n = 0$, *the black dots are the second overtone* $n = 1$, *and the red dots are the third overtone* $n = 2$.

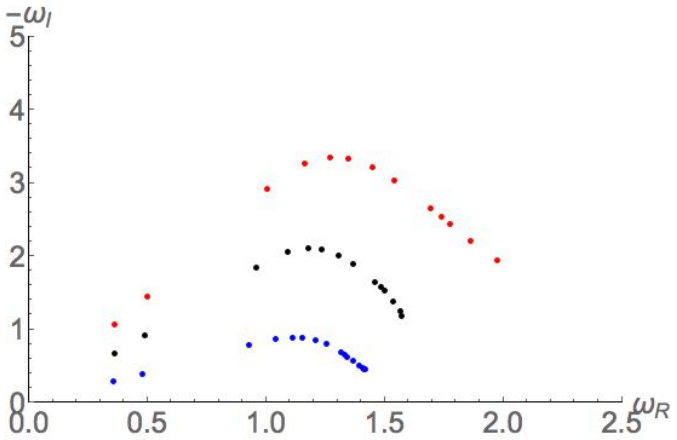

Figure 2.3 *The imaginary and real parts of the quasinormal modes for various values of the parameter* $\mu A = (0.04, 0.0625, 0.16, 0.25, 0.36, 0.49, 0.64, 0.81, 1, 2.25, 4, 9, 12.25, 25)$*, when* $\Lambda = 1$ *and* $\hat{m} = 1$*. The blue dots are the first overtone* $n = 0$*, the black dots are the second overtone* $n = 1$*, and the red dots are the third overtone* $n = 2$*.*

the parameter λ corresponds to the separation between the UV and IR cutoff scales of the conjectured dual theory–if λ becomes too large, this separation becomes too small and the braneworld black hole is no longer well represented by a quantum field theory on a BTZ black hole background.

For the region of large μA, we find that ω_I depends linearly on $\sqrt{M}$, as shown in Figure 2.6. The real part ω_R of the quasinormal modes seem to be almost independent of $\sqrt{M}$, with a small dependence appearing as μA approaches the critical turnaround point between large μA and small μA so that ω_R decreases with $\sqrt{M}$, as shown in Figure 2.7. Moreover, if we look at the spacing between the overtones of ω_I, we can numerically fit a straight line to the dependence of ω_I on $\sqrt{M}$ and find the following for the first three overtones (specific results are given for the case $\Lambda = 0.001$ and $\hat{m} = 1$):

$$n = 0 \qquad -\omega_I = 0.00 + 0.047\sqrt{M} \tag{2.28}$$

$$n = 1 \qquad -\omega_I = 0.00 + 0.11\sqrt{M} \tag{2.29}$$

$$n = 2 \qquad -\omega_I = 0.00 + 0.19\sqrt{M}. \tag{2.30}$$

2.4 Comparisons to a three-dimensional theory

We would now like to compare our results to the quasinormal modes of a three-dimensional theory. This is different from the usual approach in using quasinormal modes to investigate dualities between higher and lower-dimensional theories, wherein the quasinormal modes of the higher-dimensional theory are dual to the poles of the retarded Green's functions of a strongly-coupled CFT on the boundary in the lower-dimensional dual. Here, instead of trying to find a duality, we are comparing the phenomenology of two theories

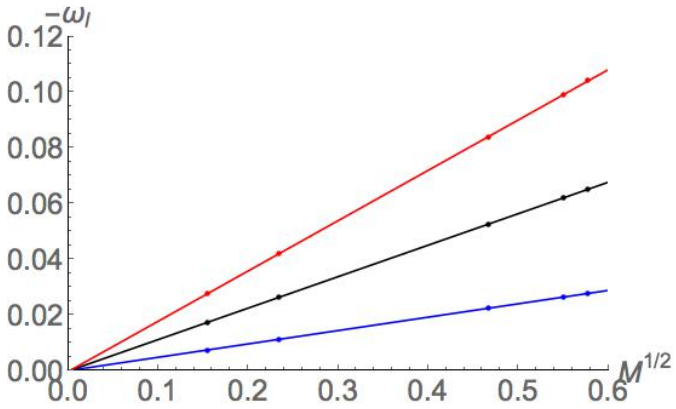

Figure 2.4 *The overtones of the imaginary part ω_I of the quasinormal modes for the 4-dimensional braneworld black holes, and their dependence on $\sqrt{M}$ where M is the mass of the black hole, in the region of small μA less than 0.33. These results are for angular momentum quantum number $\hat{m} = 1$, the lowest value of the angular quantum number K, and $\Lambda = 0.001$. The overtones correspond thus: blue ($n = 0$), black ($n = 1$), red ($n = 2$). Linear best fit lines have been drawn.*

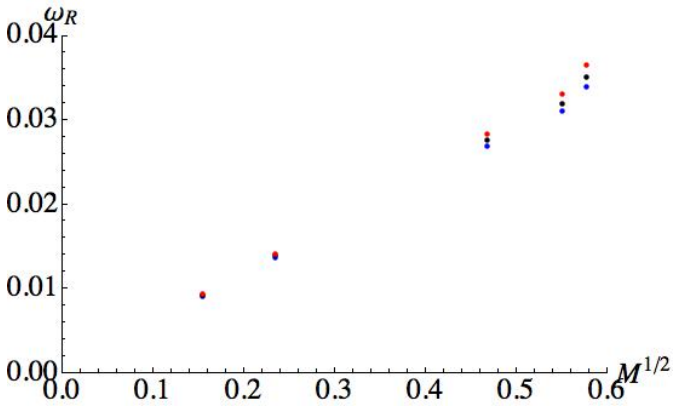

Figure 2.5 *The overtones of the real part ω_R of the quasinormal modes for the 4-dimensional braneworld black holes, and their dependence on $\sqrt{M}$ where M is the mass of the black hole, in the region of small μA less than 0.33. These results are for angular momentum quantum number $\hat{m} = 1$, the lowest value of the angular quantum number K, and $\Lambda = 0.001$. The overtones correspond thus: blue ($n = 0$), black ($n = 1$), red ($n = 2$).*

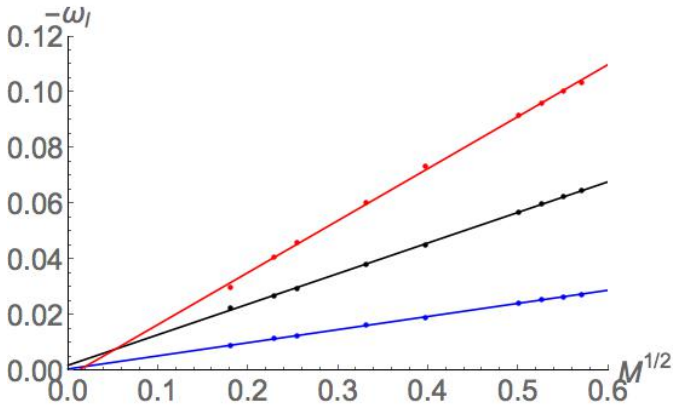

Figure 2.6 *The overtones of the imaginary part ω_I of the quasinormal modes for the 4-dimensional braneworld black holes, and their dependence on $\sqrt{M}$ where M is the mass of the black hole, in the region of large μA greater than 0.33. These results are for angular momentum quantum number $\hat{m} = 1$, the lowest value of the angular quantum number K, and $\Lambda = 0.001$. The overtones correspond thus: blue ($n = 0$), black ($n = 1$), red ($n = 2$). Linear best fit lines have been drawn.*

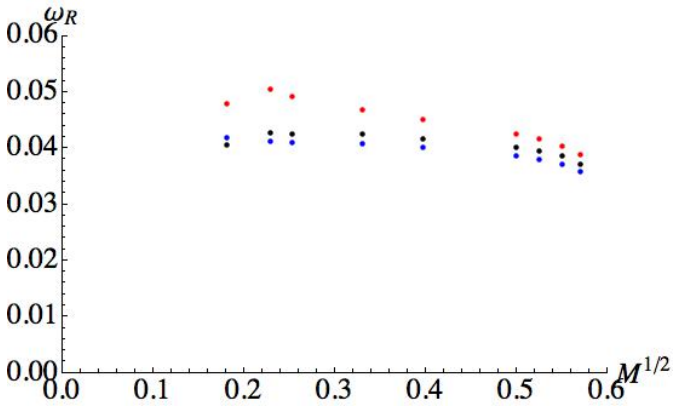

Figure 2.7 *The overtones of the real part ω_R of the quasinormal modes for the 4-dimensional braneworld black holes, and their dependence on $\sqrt{M}$ where M is the mass of the black hole, in the region of large μA greater than 0.33. These results are for angular momentum quantum number $\hat{m} = 1$, the lowest value of the angular quantum number K, and $\Lambda = 0.001$. The overtones correspond thus: blue ($n = 0$), black ($n = 1$), red ($n = 2$).*

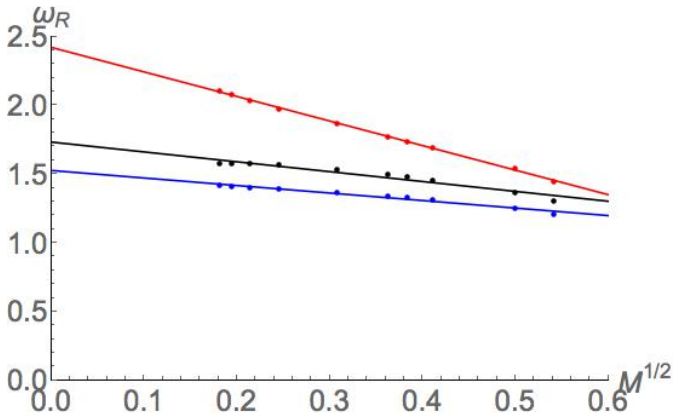

Figure 2.8 *The overtones of the real part ω_R of the quasinormal modes for the 4-dimensional braneworld black holes, and their dependence on $\sqrt{M}$ where M is the mass of the black hole, in the region of large μA greater than 0.33. These results are for angular momentum quantum number $\hat{m} = 1$, the lowest value of the angular quantum number K, and $\Lambda = 1$. The overtones correspond thus: blue ($n = 0$), black ($n = 1$), red ($n = 2$). Linear best fit lines have been drawn.*

that we know from the outset to be different: the higher-dimensional braneworld theory, and a purely lower-dimensional theory. We want to know if non-linear gravitational effects allow us to distinguish between the two theories, and to what extent. We do so by comparing the quasinormal modes of the three-dimensional black hole solution, and the quasinormal modes of the full four-dimensional braneworld solution.

It is a known result that the quasinormal mode frequencies of a massless, minimally (not conformally) coupled scalar field in a BTZ black hole background take the form [16]

$$\omega L = \pm \hat{m} - 2i(n+1)\frac{\sqrt{M}}{L}, \tag{2.31}$$

where $\hat{m}$ is the angular momentum quantum number for the $\hat{\phi}$ coordinate and n is the overtone number. Note that the real part of ω does not depend on the size of the black hole, only the imaginary part does.

The QNM of a massless, conformally coupled scalar field on a BTZ background have been previously computed in [48]. For Dirichlet boundary conditions, they are given by the values of ν for which the modified Bessel function of the first kind, $I_\nu(Z_0) = 0$, where ν is related to the QNM frequencies ω by the cosmological constant Λ and the black hole mass M, and Z_0 is given in terms of Λ, M, and also the angular momentum quantum number $\hat{m}$ of the massless, conformally coupled scalar field ϕ. The relations are as follows:

$$\nu = \frac{-i\omega}{\sqrt{\Lambda M}} \tag{2.32}$$

$$Z_0 = \sqrt{\frac{V_0}{\Lambda M}} \tag{2.33}$$

$$V_0 = |\Lambda|(4\hat{m}^2 + M) \tag{2.34}$$

The roots of $I_\nu(Z_0)$ may be found by numerical search. There are infinitely many such roots in the complex plane, giving rise to the overtones of ω. We found the roots by making contour plots of $|I_\nu(Z_0)|$ in the complex plane, searching by eye for local minima, and then doing a numerical search for the locations of the local minima. We thus obtained tables of the first six overtones of ω for $\hat{m} \in \{0, 1, 2\}$ and the values of M and Λ for which we have computed the quasinormal mode frequencies for the four-dimensional braneworld black holes. For both the minimally and conformally coupled scalar field, we find that ω_I varies linearly with $\sqrt{M}$. However, for the minimally coupled scalar field, ω_R depends only on $\hat{m}$, whereas for the conformally coupled scalar field, ω_R decreases linearly with $\sqrt{M}$.

Comparing these known results to the quasinormal mode frequencies for a conformally coupled scalar field propagating on the background of a four-dimensional braneworld black hole, as obtained in Section 2.3, we find that there is no obvious correspondence between the ω_R in the region of small μA, to the quasinormal mode frequencies for the three-dimensional theory. There is, however, a similarity between ω_R in the region of large μA, and the quasinormal mode frequencies of the conformally coupled scalar field on a BTZ black hole background. In both cases, ω_R decreases with $\sqrt{M}$, though the linear dependence is far more obvious in the case of the scalar field in the three-dimensional BTZ black hole background. The difference between the trends in ω_R is most likely due to the strongly coupled nature of the theory dual to the four-dimensional braneworld solution.

When it comes to the imaginary parts of the quasinormal mode frequencies, in the case of both large and small values of μA, ω_I not only depends linearly on $\sqrt{M}$, the overtones of the conformally coupled scalar field on the braneworld black hole background, can be rescaled by a constant factor to match the overtones of the conformally coupled

scalar field on the BTZ black hole background. The correspondence is not one-to-one: namely, the $n = 0, 1, 2$ overtones of the four-dimensional quasinormal modes map to the $n = 0, 2, 4$ overtones of the BTZ quasinormal modes. Note that the existence of such a phenomenological similarity is by no means a given. It indicates that the overtones of the quasinormal modes, or at least their imaginary parts, for the two theories have the same functional dependence on the overtone number n and the quantity $\sqrt{M}$, so that the two theories are phenomenologically similar. This property has been confirmed for the first three overtones when $\hat{m} = 0$, and the first two overtones when $\hat{m} = 1$. It remains to be seen if the quasinormal mode frequencies can be computed to sufficient accuracy to see if the correspondence persists for higher overtones (which will nevertheless be muted in effect compared to the first few dominant overtones.)

2.5 Discussion

We find evidence for an interesting possible phenomenological similarity between the full four-dimensional braneworld theory and a purely three-dimensional theory. The quasinormal modes of a massless, conformally coupled scalar field on the full four-dimensional braneworld black hole background have a similar dependence on the quantity $\sqrt{M}$ where M is the mass of the black hole–which is equal in both the three and four-dimensional sense–as do the quasinormal modes of a massless, conformally coupled scalar field on the three-dimensional BTZ black hole background. As these calculations take into account the full non-linear dynamics of the fields when coupled to gravity, this correspondence indicates that the theories may be indistinguishable even at the nonlinear level. However, this

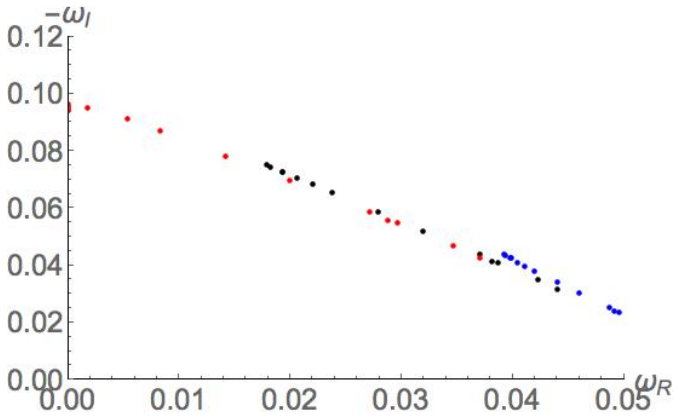

Figure 2.9 *The imaginary and real parts ω_I and ω_R of the quasinormal modes of a BTZ black hole perturbed by a massless conformal scalar field. These results are for angular momentum quantum number $\hat{m} = 1$, $\Lambda = 0.001$, and the mass M of the BTZ black hole ranging between $M = 0.024$ and $M = 0.33$. The overtones correspond thus: blue ($n = 0$), black ($n = 1$), red ($n = 2$). Linear best fit lines have been drawn.*

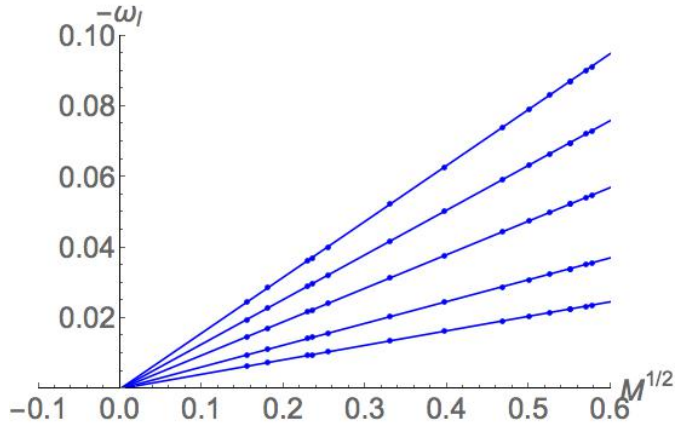

Figure 2.10 *The overtones of the imaginary part ω_I of the quasinormal modes for a BTZ black hole perturbed by a massless conformal scalar field, and their dependence on $\sqrt{M}$ where M is the mass of the black hole. These results are for angular momentum quantum number $\hat{m} = 0$, and $\Lambda = 0.001$. The first six overtones have been plotted, and $|\omega_I|$ increases with increasing overtone number n. Linear best fit lines have been drawn.*

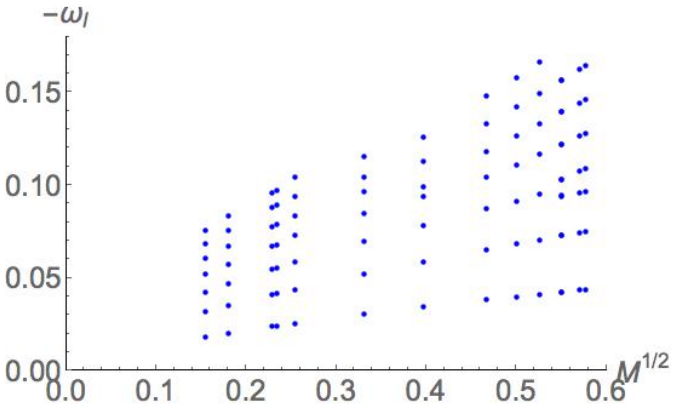

Figure 2.11 *The overtones of the imaginary part ω_I of the quasinormal modes for a BTZ black hole perturbed by a massless conformal scalar field, and their dependence on $\sqrt{M}$ where M is the mass of the black hole. These results are for angular momentum quantum number $\hat{m} = 1$, and $\Lambda = 0.001$. The first eight overtones have been plotted, and $|\omega_I|$ increases with increasing overtone number n. We can see that there is an interesting bifurcation structure in ω_I.*

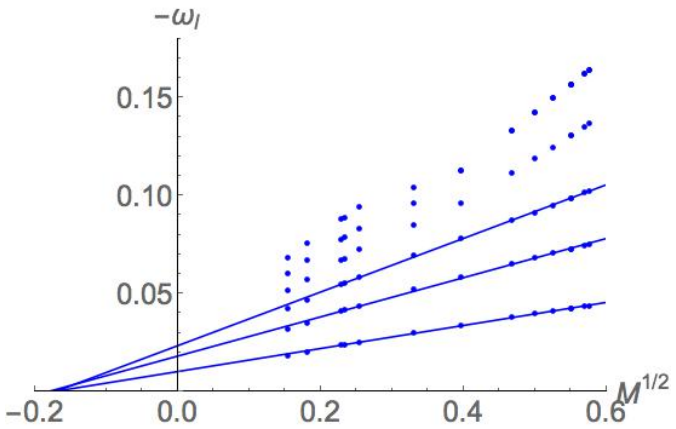

Figure 2.12 *The overtones of the imaginary part ω_I of the quasinormal modes for a BTZ black hole perturbed by a massless conformal scalar field, and their dependence on $\sqrt{M}$ where M is the mass of the black hole. These results are for angular momentum quantum number $\hat{m} = 1$, and $\Lambda = 0.001$. The first eight overtones have been plotted, and $|\omega_I|$ increases with increasing overtone number n. The bifurcated structure of ω_I has been taken into account in order to draw linear best fit lines for the first three overtones.*

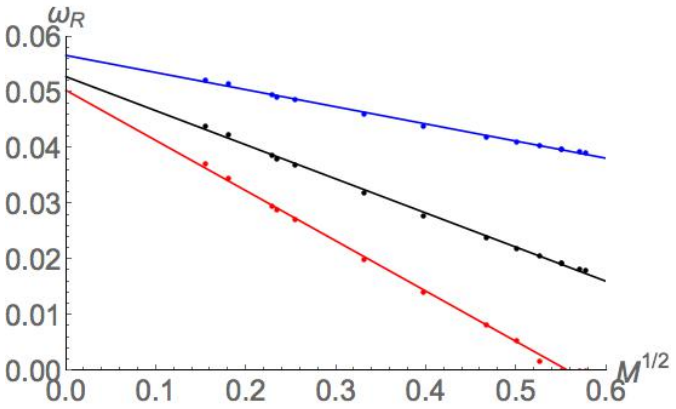

Figure 2.13 *The overtones of the real part ω_R of the quasinormal modes for a BTZ black hole perturbed by a massless conformal scalar field, and their dependence on $\sqrt{M}$ where M is the mass of the black hole. These results are for angular momentum quantum number $\hat{m} = 1$, and $\Lambda = 0.001$. The first three overtones have been plotted, and correspond thus: blue ($n = 0$), black ($n = 1$), red ($n = 2$). Linear best fit lines have been drawn.*

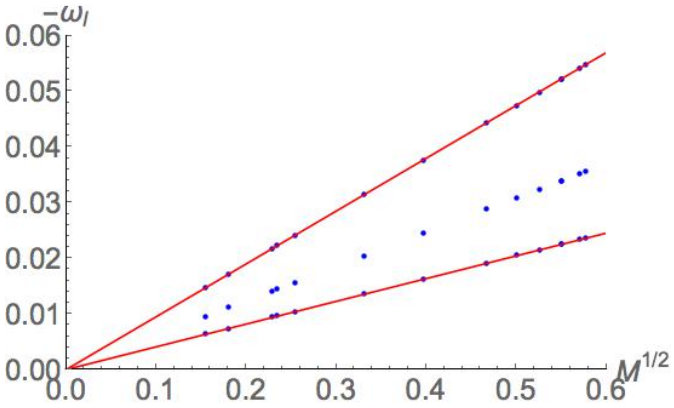

Figure 2.14 *The scaling of the first two overtones ($n = 0$ and $n = 1$) of ω_I of the 4-dimensional braneworld black hole to fit the first ($n = 0$) and third ($n = 2$) overtones of the BTZ black hole perturbed by a massless conformal scalar field, when the angular momentum quantum number $\hat{m} = 0$. The blue dots are the quasi normalmodes of the BTZ black hole, and the red lines are lines of best fit to the scaled quasinormal modes of the 4-dimensional black hole. Scaling $\omega_I \to 0.87\omega_I$ maps the first set of quasinormal modes to the second set.*

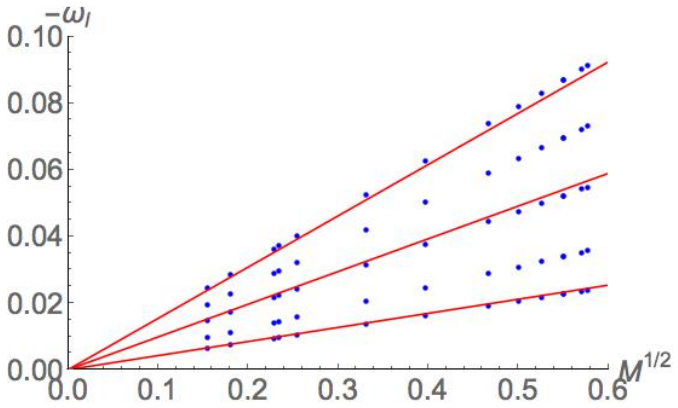

Figure 2.15 *The scaling of the first three overtones ($n = 0, 1, 2$) of ω_I of the 4-dimensional braneworld black hole to fit the first ($n = 0$), third ($n = 2$), and fifth ($n = 4$) overtones of the BTZ black hole perturbed by a massless conformal scalar field, when the angular momentum quantum number $\hat{m} = 0$. The blue dots are the quasi normalmodes of the BTZ black hole, and the red lines are lines of best fit to the scaled quasinormal modes of the 4-dimensional black hole. Scaling $\omega_I \to 0.9\omega_I$ maps the first set of quasinormal modes to the second set, though the mapping is less exact than when only the first two overtones of the braneworld black hole are considered.*

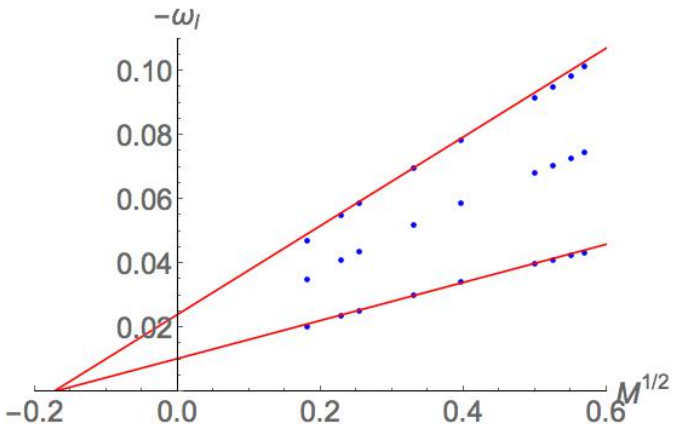

Figure 2.16 *The scaling of the first two overtones ($n = 0$ and $n = 1$) of ω_I of the 4-dimensional braneworld black hole to fit the first ($n = 0$) and third ($n = 2$) overtones of the BTZ black hole perturbed by a massless conformal scalar field, when the angular momentum quantum number $\hat{m} = 1$. The blue dots are the quasi normalmodes of the BTZ black hole, and the red lines are lines of best fit to the scaled quasinormal modes of the 4-dimensional black hole. Scaling $\omega_I \to 1.258\omega_I$ maps the first set of quasinormal modes to the second set.*

similarity only holds for ω_I–the real parts ω_R of the quasinormal modes have a different dependence on M in the higher-dimensional theory, than in the lower-dimensional case. Moreover, although ω_I depends linearly on $\sqrt{M}$, similarly to the case of the scalar fields propagating on the BTZ black hole backgorund, the overtones of ω_I cannot be mapped by a simple one-to-one scaling onto the overtones of ω_I in the three-dimensional theory. Thus, although there are similarities between the observables in the two theories, these results indicate that sufficient sensitivity in measuring observables will at some point allow non-linear gravitational effects to tell the two apart.

Chapter 3

Evolution of Near-Extremal Black Holes in $\mathcal{N} = 2$, $d = 4$ Supergravity

In this chapter we investigate the stability of a near-extremal D0-D4 black hole in the probe limit, when the parameters of the black hole solution lie within a certain regime, as a precursor to studying the bound states of multiple non-extremal black holes in $\mathcal{N} = 2$, $d = 4$ supergravity. We determine whether it is possible to form bound states of this "core" non-extremal black hole with BPS probe particles, and whether it is possible for the "core" black hole to decay by the emission of such BPS probes either to a local minimum of the probe potential, or spatial infinity. We first carry out a qualitative analysis of the probe potential to determine when quantum tunneling of probes from the black hole is possible. We then find the wavefunction of the scattered probe by using the WKB approximation to solve the Dirac equation in the black hole background, and use this solution to compute the tunneling amplitude.

In Section 3.1 we define the problem we are trying to solve and introduce some motivation for working on the problem. In Section 3.2 we introduce the background information necessary to understand the work in this Chapter. In Section 3.3 we present our results. In Section 3.2.2 we give the action for a charged probe particle in this black hole background, and carry out a qualitative analysis of the static probe potential. In Section 3.3.3 we set out the Dirac equation in the black hole background, and in Section 3.3.5 we carry out the full tunneling analysis by solving the Dirac equation. We conclude in Section 4.4.

3.1 Introduction

A class of black holes that has not been extensively studied so far consists of the non-extremal black hole solutions to $\mathcal{N} = 2$, $d = 4$ supergravity [76, 78, 79], that are a generalization of the well-known extremal (both BPS and non-BPS) "attractor" solutions [81]. These solutions consist of the background metric, together with a set of complex scalars and electromagnetic gauge fields, and can be completely characterized by the black hole's electric and magnetic charges, the parameter c giving the deviation from extremality, and the value of the scalars at spatial infinity. In this work we study a particular class of these black hole solutions that have one electric charge Q_0, one magnetic charge P_1, and one complex scalar field. Thus these solutions can be specified by four independent quantities: Q_0, P_1, the extremality parameter c, and the value of the scalar field at spatial infinity. We package these quantities into two parameters, $\frac{1}{\tilde{c}_2}$ and $\frac{1}{\tilde{c}_4}$, that we use to classify the various regimes in which these solutions lie.

The BPS attractor solutions are known to exist in multi-centered configurations that are stable bound states [84, 86]. These multicentered configurations should remain valid, stable solutions even when deformed away from extremality [79], but fully backreacted, non-extremal, multicentered solutions have not yet been found. As the probe limit of BPS particles in a single-centered BPS background gives interesting insights into the fully backreacted supersymmetric multicentered solutions (such as the equilibrium distance between the centers) [84–86], it is reasonable to assume that studying the behavior of BPS probes in the background of a single-centered non-extremal black hole should provide clues to the existence and stability of multi-centered non-extremal black hole solutions.

We thus consider a central "core" non-extremal black hole, that can be surrounded by BPS probes (in a multi-centered configuration with a large black hole at the center and the remaining black holes being small enough relative to the "core" black hole that they can be treated as BPS probes), and study the static potential of the probes in the black hole background. We assume that the probes are small enough that mutual interactions between them can be ignored. If the probe potential has a local minimum whose free energy is lower than that of the free energy at the black hole horizon, then the probe can form a stable bound state with the background black hole [79, 80] (and when fully back-reacted, this could give a bound state of two black holes.) A single black hole whose charge is equal to the sum of the "core" charge and the probe charge is unstable to the emission of such a probe to form this bound state, as the probe can tunnel through the potential barrier to the local minimum of the potential. If the probe has a lower free energy at spatial infinity than it does at the black hole horizon, then the "core" black hole is unstable, as it can emit probes that can tunnel through the potential barrier to escape to infinity. We cannot

predict the endpoint of this evolution, as at some point the probe approximation (where the interaction between the probes is negligible) will become inapplicable: however, it is possible that the "core" black hole will continue to emit probes to infinity until we are left with a hot dilute gas.

In this chapter we consider the emission of such charged probes from a certain class of non-extremal black holes in the near-extremal case, where the parameters describing the black hole solutions satisfy $c \lll \frac{1}{\tilde{c}_2} \sim \frac{1}{\tilde{c}_4}$. We would like to know if these black holes are unstable to the emission of charged BPS probes, and if so, to determine whether these probes can form bound states with the background black hole, and to compute the tunneling amplitudes for this emission process. We first study the qualitative features of the potential for a static charged probe in the black hole background, finding the maximum of the potential and the classical turning points. We also compute the rate for a charged particle to tunnel through the static potential between the classical turning points. This naive result for the tunneling rate through the potential barrier may also be applied to the case where the parameters of the black hole solution satisfy $c \lll \frac{1}{\tilde{c}_2} \lll \frac{1}{\tilde{c}_4}$.

We then find the wavefunction for a charged probe particle in the black hole background, by solving the curved space Dirac equation for this background. We use the WKB approximation to solve for the radial part of the wavefunction. We then compute the amplitude for a charged probe particle to be emitted from the black hole via quantum tunneling through the potential barrier, by calculating the ratio of the conserved current density at spatial infinity and at the black hole horizon.

3.2 Background Information

3.2.1 Non-extremal black holes in $\mathcal{N} = 2$, $d = 4$ supergravity

The action for the bosonic part of four-dimensional $\mathcal{N} = 2$ supergravity coupled to massless vector multiplets takes the form:

$$S_{4D} = \frac{1}{16\pi} \int_{M_4} d^4x \sqrt{-g} \left(R - 2G_{A\bar{B}} dz^A \wedge \star d\bar{z}^{\bar{B}} - F^I \wedge G_I \right), \tag{3.1}$$

where the z^A $(A = 1, \ldots, n)$ are the vector multiplet scalars, the F^I $(I = 0, 1, \ldots, n)$ are the vector field strengths, the G_I are the dual magnetic field strengths, and $G_{A\bar{B}} = \partial_A \partial_{\bar{B}} \mathcal{K}$ is derived from the Kahler potential

$$\mathcal{K} = -\ln(i \int_X \Omega_0 \wedge \bar{\Omega}_0) \tag{3.2}$$

where Ω_0 is the holomophic 3-form on the Calabi-Yau manifold X. The normalized 3-form $\Omega = e^{\mathcal{K}/2}\Omega_0$.

The lattice of electric and magnetic charges Γ is identified with $H^3(X, \mathbb{Z})$, the lattice of integral harmonic 3-forms on X. In the standard symplectic basis, a charge Γ can be written as $\Gamma = (P^I, Q_I)$, with magnetic charges P^I and electric charges Q_I. We can define a canonical, duality invariant, symplectic product $\langle , \rangle$ on the space of charges, which is given by:

$$\langle \Gamma, \tilde{\Gamma} \rangle = P^I \tilde{Q}_I - Q_I \tilde{P}^I \tag{3.3}$$

in the standard symplectic basis. The moduli-dependent central charge $Z(\Gamma, z)$ of Γ is given by:

$$Z(\Gamma, z) = -e^{\mathcal{K}/2} \langle \Gamma, \Omega \rangle \tag{3.4}$$

All the coefficients of the Lagrangian can be derived from a single prepotential $F(X)$, where the X^A are projective coordinates such that $X^A = X^0 z^A$ and X^0 is a gauge degree of freedom. In this work we will consider prepotentials of the form:

$$F(X) = D\frac{(X^1)^3}{6X^0}, \tag{3.5}$$

with $D = 1$, so that we have one scalar field, z, and two electromagnetic vector potentials, A^0 and A^1 (together with their duals, B^0 and B^1.) In this case the moduli-dependent central charge for a charge $\gamma = (P^0, P^1, Q_1, Q_0)$ is given explicitly by:

$$Z(\gamma, z) = \frac{\sqrt{3}}{2\sqrt{D(\mathrm{Im}z)^3}}\left(\frac{D}{6}P^0 z^3 - \frac{D}{2}P^1 z^2 + Q_1 z + Q_0\right) \tag{3.6}$$

This restriction still allows us to consider a large class of black hole solutions, as it has been shown that the general case with an arbitrary number of n vector multiplets may be reduced to an effective theory with a single vector multiplet given by the prepotential (3.5), by applying a suitable truncation [77].

The Black Hole Solution

Non-extremal black hole solutions to this theory were first found in [76] and [78], and further studied in [79] and [80]. We consider the D0-D4 solutions of D0-charge Q_0 and D4-charge P_1, which may be described by a charge vector $\Gamma = (P^1, Q_0)$. In analogy with the well-known extremal black hole solutions [81], a non-extremal solution can be given in terms of two functions H_0, H_1:

$$H_0 \equiv \frac{|Q_0|}{c}\sinh(c\tau + c_2), \qquad H_1 \equiv \frac{|P_1|}{c}\sinh(c\tau + c_4) \tag{3.7}$$

where c_2 and c_4 are constants, c denotes the deviation from extremality, and τ is an inverse radial coordinate such that $\tau \to \infty$ at the black hole horizon and $\tau \to 0$ at spatial infinity

(in the extremal limit, the functions H_0, H_1 are harmonic.) If Q_0 and P_1 are both positive, then the solution is BPS in the extremal limit $c \to 0$. If Q_0 and P_1 have differing sign (where without loss of generality we can take $Q_0 < 0$), then the solution is non-BPS in the extremal limit. In this work we will restrict ourselves to the near-extremal regime where $c \lll \frac{1}{c_2}$ and $c \lll \frac{1}{c_4}$.

The black hole metric is given by [78, 79]:

$$ds^2 = -e^{2U(\tau)}dt^2 + e^{-2U(\tau)}\left(\frac{c^4}{\sinh^4 c\tau}d\tau^2 + \frac{c^2}{\sinh^2 c\tau}d\Omega_2^2\right) \tag{3.8}$$

where

$$e^{-2U} = \sqrt{\frac{2}{3}H_0 H_1^3}. \tag{3.9}$$

The scalar field $z = iy$ is given by:

$$y = \sqrt{\frac{6H_0}{H_1}}, \tag{3.10}$$

and the electromagnetic vector potentials are given by:

$$\begin{aligned} A^0 &= \frac{1}{2Q_0}\left(\sqrt{c^2 + \frac{Q_0^2}{H_0^2}} - c\right)dt, \qquad A^1 = P_1(1-\cos\theta)d\phi \\ B_0 &= Q_0(1-\cos\theta)d\phi, \qquad B_1 = -\frac{3}{2P_1}\left(\sqrt{c^2 + \frac{P_1^2}{H_1^2}} - c\right)dt. \end{aligned} \tag{3.11}$$

The integration constants c_2 and c_4 are given by:

$$\sinh c_2 = \frac{c y_0^{3/2}}{2\sqrt{3}|Q_0|}, \qquad \sinh c_4 = \frac{\sqrt{3}c}{|P_1| y_0^{1/2}}, \tag{3.12}$$

where y_0 is the value of the scalar field at spatial infinity. Note that the solution is completely determined by the charges (P^1, Q_0), the extremality parameter c, and the value

y_0 of the scalar field at spatial infinity. Thus four independent parameters are needed to specify the solution. In the rest of this work we will refer to the parameters (P^1, Q_0), c, c_2, and c_4, but it should be kept in mind that one of these is redundant.

We will find it convenient to define the parameters:

$$\tilde{c}_2 \equiv \frac{\sinh c_2}{c}, \qquad \tilde{c}_4 \equiv \frac{\sinh c_4}{c} \tag{3.13}$$

The ADM mass M of the black hole can be read off from the metric:

$$M = \frac{1}{4}\sqrt{c^2 + \frac{12Q_0^2}{y_0^3}} + \frac{3}{4}\sqrt{c^2 + \frac{P_1^2 y_0}{3}} \tag{3.14}$$

where y_0 is the value of y at spatial infinity. The entropy of the black hole is:

$$S = \pi \left(c + \sqrt{c^2 + \frac{12Q_0^2}{y_0^3}} \right)^{1/2} \left(c + \sqrt{c^2 + \frac{P_1^2 y_0}{3}} \right)^{3/2} \tag{3.15}$$

and the Hawking temperature is:

$$T_H = \frac{c}{2S} \tag{3.16}$$

In this work we will use the radial coordinate r defined by:

$$r \equiv \frac{c}{\sinh c\tau} \tag{3.17}$$

In these coordinates the metric becomes:

$$ds^2 = -e^{2U(r)}dt^2 + e^{-2U(r)} \left(\frac{1}{\left(1 + \frac{c^2}{r^2}\right)} dr^2 + r^2 d\Omega_2^2 \right) \tag{3.18}$$

And the functions determining the solutions are:

$$H_0 = |Q_0| \left(\frac{\cosh c_2}{r} + \tilde{c}_2 \sqrt{1 + \frac{c^2}{r^2}} \right), \qquad H_1 = |P_1| \left(\frac{\cosh c_4}{r} + \tilde{c}_4 \sqrt{1 + \frac{c^2}{r^2}} \right) \tag{3.19}$$

3.2.2 The Probe Action

Before solving for the wavefunction of a BPS particle of charge γ in the black hole background, it will be helpful to study the probe action for such a particle in this background, which is given by [83]:

$$S_\gamma = -\int \mu \, \mathrm{d}s - \frac{1}{2}\int \langle \gamma, \mathbb{A}_\mu \rangle \mathrm{d}x^\mu \tag{3.20}$$

where μ is the moduli-dependent mass of the particle, given by:

$$\mu = |Z(\gamma, z)| \tag{3.21}$$

The *static* probe action is:

$$\begin{aligned} S_p &= -\int \mu \sqrt{-g_{tt}} \, \mathrm{d}t - \frac{1}{2}\int \langle \gamma, \mathbb{A}_t \rangle \mathrm{d}t \\ &= \int V_p \, \mathrm{d}t \end{aligned} \tag{3.22}$$

where V_p is the static probe potential. This can be written in the form $V_p = V_g + V_{\mathrm{em}}$, where $V_g = e^U |Z(\gamma, z)|$ is the mass term, given by [79]:

$$V_g = \frac{1}{4}\sqrt{\left(\frac{q_0}{H_0} + \frac{3p_1}{H_1}\right)^2 + \frac{6H_0}{H_1}\left(\frac{q_1}{H_0} - \frac{p_0}{H_1}\right)^2}, \tag{3.23}$$

and V_{em} is the electromagnetic coupling term, given by:

$$V_{\mathrm{em}} = -\frac{1}{4}\frac{q_0}{Q_0}\left(\sqrt{c^2 + \frac{Q_0^2}{H_0^2}} - c\right) - \frac{3}{4}\frac{p_1}{P_1}\left(\sqrt{c^2 + \frac{P_1^2}{H_1^2}} - c\right). \tag{3.24}$$

We can read off the electromagnetic vector potential for this configuration from the full (i.e. non-static) probe action (3.20):

$$\begin{aligned} A_t &= -\frac{1}{4}\frac{q_0}{Q_0}\left(\sqrt{c^2 + \frac{Q_0^2}{H_0^2}} - c\right) - \frac{3}{4}\frac{p_1}{P_1}\left(\sqrt{c^2 + \frac{P_1^2}{H_1^2}} - c\right) \\ A_\phi &= \frac{\langle \gamma, \Gamma \rangle}{2}(1 - \cos\theta) \end{aligned} \tag{3.25}$$

3.3 Results

3.3.1 Qualitative Analysis of the Probe Potential

In this section we carry out a qualitative analysis of the static probe potential in the near-extremal regime $c \lll \frac{1}{\tilde{c}_2}, \frac{1}{\tilde{c}_4}$. We will find it useful to define the following quantities:

$$A_1 \equiv \frac{1}{4}\frac{q_0}{Q_0} + \frac{3}{4}\frac{p_1}{P_1} \tag{3.26}$$

$$E_0 \equiv \sqrt{\frac{2}{3}|Q_0||P_1|^3} \tag{3.27}$$

$$\mu_0^2 \equiv |Z(\gamma,z)|^2_{r\lll\frac{1}{\tilde{c}_2}} = \frac{E_0}{16}\left[\left(\frac{q_0}{|Q_0|}+\frac{3p_1}{|P_1|}\right)^2 + \frac{6|Q_0|}{|P_1|}\left(\frac{q_1}{|Q_0|}-\frac{p_0}{|P_1|}\right)^2\right] \tag{3.28}$$

$$\mu_\infty^2 \equiv |Z(\gamma,z)|^2_{r\to\infty} = \frac{1}{16}\left[\left(\frac{q_0}{\tilde{c}_2|Q_0|}+\frac{3p_1}{\tilde{c}_4|P_1|}\right)^2 + \frac{6|Q_0|\tilde{c}_2}{|P_1|\tilde{c}_4}\left(\frac{q_1}{\tilde{c}_2|Q_0|}-\frac{p_0}{\tilde{c}_4|P_1|}\right)^2\right] \tag{3.29}$$

We will carry out a full scattering analysis only in the case where $\frac{1}{\tilde{c}_2} \sim \frac{1}{\tilde{c}_4}$, which allows the calculations to be simplified. Note that in this case we have $\mu_0^2 \sim \mu_\infty^2$, and $E_0 \sim \frac{1}{\tilde{c}_2^2}$.

The probe has zero potential energy at the horizon $r = 0$, while its potential energy at spatial infinity is

$$V_p|_{r=\infty} = \mu_\infty - \frac{1}{4}\frac{q_0}{Q_0\tilde{c}_2} - \frac{3}{4}\frac{p_1}{P_1\tilde{c}_4} + cA_1 \tag{3.30}$$

$$= \mu_\infty - A_1(E_0^{\frac{1}{2}} - c) \tag{3.31}$$

Tunneling of a probe particle to spatial infinity is only possible if this potential energy is non-positive, so that $\mu_\infty \leq A_1(E_0^{\frac{1}{2}} - c)$ (note that $E_0^{\frac{1}{2}} \sim 1/\tilde{c}_2 >>> c$, so that in order for tunneling to spatial infinity to be allowed, we must have $A_1 > 0$.) We can see from (3.25) that the intersection product $\langle\gamma,\Gamma\rangle$ between the probe and the black hole determines

the magnetic part of the vector potential, not the electrostatic part: so the sign of the intersection product is independent of the sign of the static potential at spatial infinity.

From (3.26)-(3.27) and (3.29) we see that if the black hole is BPS in the extremal limit, then $V_p|_{r=\infty} > 0$ unless the extremality parameter $c = 0$ and the intersection product $\langle \gamma, \Gamma \rangle$ between the probe charge γ and the black hole charge Γ is zero, in which case $V_p|_{r=\infty} = 0$. In all other cases, the emission and absorption of probes is infinitely suppressed from black holes that are BPS in the extremal limit. Thus, apart from the special case of the emission of probe particles with $\langle \gamma, \Gamma \rangle = 0$ from BPS black holes, we are only considering the scattering of probes from black holes that are non-BPS in the extremal limit. This result is very natural, as the fully backreacted, two-centered BPS black hole solution has an angular momentum proportional to $\langle \Gamma_1, \Gamma_2 \rangle$ where Γ_1 and Γ_2 are the charges of the two black holes, whereas a single-centered BPS black hole has zero angular momentum [84–86]. Thus, if $\langle \gamma, \Gamma \rangle \neq 0$, then emission of the probe γ from the background black hole is forbidden by conservation of angular momentum in the extremal limit, when the background black hole is BPS.

We can study the shape of V_p in the two regions $r \lll \frac{1}{\tilde{c}_2}$ and $r \ggg c$. For $r \lll \frac{1}{\tilde{c}_2}$ we have:

$$V_p|_{r \lll \frac{1}{\tilde{c}_2}} = \frac{r}{E_0^{\frac{1}{2}}} \mu_0 - c A_1 \left(\sqrt{1 + \frac{r^2}{c^2}} - 1 \right) \tag{3.32}$$

Solving $\frac{\partial V_p}{\partial r}|_{r=r_0} = 0$ gives:

$$r_0 = c \sqrt{\frac{1}{\alpha_0^2} - 1} \tag{3.33}$$

where

$$\alpha_0^2 \equiv 1 - \frac{\mu_0^2}{A_1^2 E_0}. \tag{3.34}$$

Since $V''(r_0) < 0$, this is a maximum of the potential. And since $\mu_\infty \leq A_1(E_0^{\frac{1}{2}} - c)$ when emission to infinity is allowed, and $\mu_\infty^2 = \mu_0^2$, we have the following lower bound on α_0^2 (remembering that we are in the near-extremal regime $c\tilde{c}_2 \lll 1$):

$$\alpha_0^2 \geq \frac{A_1^2 E_0 - (A_1 E_0^{\frac{1}{2}} - cA_1)^2}{A_1^2 E_0} \tag{3.35}$$

$$\sim c\tilde{c}_2 \tag{3.36}$$

This also puts the following upper bound on r_0:

$$r_0 \leq \frac{c^{\frac{1}{2}}}{\tilde{c}_2^{\frac{1}{2}}} \lll \frac{1}{\tilde{c}_2}, \tag{3.37}$$

so we see that the maximum of the potential is indeed in the region $r \lll \frac{1}{\tilde{c}_2}$ in all the cases where emission to infinity is allowed.

In the region $r \ggg c$ we have:

$$V_p|_{r \ggg c} = \frac{r(\tilde{c}_2 \mu_\infty - A_1)}{1 + r\tilde{c}_2} + cA_1 \tag{3.38}$$

so that

$$\frac{\partial V_p}{\partial r} = \frac{\mu_\infty E_0^{-\frac{1}{2}} - A_1}{(1 + \tilde{c}_2 r)^2}, \tag{3.39}$$

which is ≤ 0 in all the cases where emission to spatial infinity is allowed. Thus we see that with $\frac{1}{\tilde{c}_2} \sim \frac{1}{\tilde{c}_4}$, the potential has one maximum at $r = r_0$ in the region $r \sim c$, then decreases continuously, tending towards the constant value $V_p(\infty) = \mu_\infty - A_1(E_0^{\frac{1}{2}} - c)$ at spatial infinity. The potential does not have a local minimum, and thus the "core" black

hole cannot form a bound state with a BPS probe. A probe that is emitted will tunnel through the potential barrier and escape to spatial infinity.

The maximum value of the potential at r_0 is given by

$$\epsilon_{\max} \equiv V_p(r_0) = cA_1(1-\alpha_0) \tag{3.40}$$

Thus we can write the energy for a general scattered/emitted low energy particle as:

$$\epsilon = cA_1(1-\beta\alpha_0) \tag{3.41}$$

where $1 \leq \beta \leq \frac{1}{\alpha_0}$. The classical turning points for this particle are:

$$r_\pm = \frac{c}{\alpha_0}\left[\beta\sqrt{1-\alpha_0^2} \pm \sqrt{\beta^2-1}\right] \tag{3.42}$$

A low energy probe particle that has Poincare energy less than or equal to the maximum value $\epsilon_{\max}$ of the potential can be emitted from the horizon, tunnel through the barrier between the classical turning points r_- and r_+, and escape to spatial infinity. Alternatively, a particle may come in from infinity and scatter off the potential, either being reflected back from the barrier, or tunneling through from the turning point r_+ to r_- before falling into the horizon. If the background black hole is BPS, then the static probe potential V_p for a probe particle with $\langle\gamma,\Gamma\rangle = 0$ is actually flat for all r, so there is no barrier to emission or absorption.

Note that V_p takes the same form as (3.32) in the region $r \lll \frac{1}{\tilde{c}_2}$ when $\frac{1}{\tilde{c}_2} \lll \frac{1}{\tilde{c}_4}$. Thus, if $\alpha_0 \leq 1$, then the probe potential in this case also has a maximum at r_0 with the same value $\epsilon_{\max}$. Although a complete scattering analysis for regions $r \ggg c$ is more complicated in this case, the tunneling rate between the turning points $r_\pm$ of this potential is the same as in the case $\frac{1}{\tilde{c}_2} \sim \frac{1}{\tilde{c}_4}$ and may be calculated in the same manner, as we will see in Section 3.3.2.

3.3.2 The Tunneling Rate Through The Probe Potential Barrier

Even without completing the full scattering calculation, we can obtain an estimate of the tunneling rate Γ_t through the potential barrier, which is defined as:

$$\Gamma_t \equiv e^{-\int_{r_-}^{r_+} |p'_r| dr'}, \tag{3.43}$$

where $r_\pm$ are the classical turning points for the probe in the static potential, and p_r is the radial canonical momentum, given by:

$$p_r \equiv \frac{\partial \mathcal{L}}{\partial \dot{r}}. \tag{3.44}$$

The Lagrangian density $\mathcal{L}$ can be found from the probe action (3.20):

$$\mathcal{L} = -\mu \sqrt{e^{2U} - \left(\frac{e^{-2U}}{1+\frac{c^2}{r^2}}\right)\dot{r}^2} - A_t, \tag{3.45}$$

where A_t is given by (3.25). This gives

$$p_r = \frac{\mu e^{-2U}\dot{r}}{\sqrt{e^{2U}\left(1+\frac{c^2}{r^2}\right)^2 - e^{-2U}\left(1+\frac{c^2}{r^2}\right)\dot{r}^2}} \tag{3.46}$$

The conserved canonical energy ϵ satisfies:

$$\epsilon = \dot{r}\frac{\partial \mathcal{L}}{\partial \dot{r}} - \mathcal{L} \tag{3.47}$$

$$= A_t + \sqrt{\left(1+\frac{c^2}{r^2}\right)e^{4U}p_r^2 + e^{2U}\mu^2} \tag{3.48}$$

Thus we find that

$$p_r^2 = \frac{e^{-4U}}{\left(1+\frac{c^2}{r^2}\right)}\left((\epsilon - A_t)^2 - e^{2U}\mu^2\right). \tag{3.49}$$

For the range of parameters that we are considering for the background black hole, the classical turning points $r_\pm$ for the scattered probe particle always lie in the region $r \lll c$. Thus, defining the coordinate $z \equiv r^2/c^2$, the classical turning points lie in the region $z \lll 1$ and are given by (3.42):

$$z_\pm = \frac{\beta^2}{\alpha_0^2}\left(\pm 1 + \sqrt{(1-\alpha_0^2)(1-\frac{1}{\beta^2})}\right)^2 - 1 \tag{3.50}$$

$$z_+ - z_- = \frac{4\beta}{\alpha_0^2}\sqrt{(1-\alpha_0^2)(\beta^2-1)} \tag{3.51}$$

We find that

$$\lim_{\zeta\to 0} |\mathrm{Re}\left(i\left[p_r(z_+-\zeta) - p_r(z_--\zeta)\right]\right)| = -a_1\alpha_0\pi(\beta-1), \tag{3.52}$$

and so

$$\Gamma_{\mathrm{t}} = e^{-a_1\alpha_0\pi(\beta-1)} \tag{3.53}$$

As mentioned at the end of Section 3.3.1, Γ_t also gives the tunneling rate through the potential barrier in the regime $\frac{1}{\tilde{c}_2} \lll \frac{1}{\tilde{c}_4}$, as the probe potential V_p has the same form in the region $r \lll \frac{1}{\tilde{c}_2}$ as when $\frac{1}{\tilde{c}_2} \sim \frac{1}{\tilde{c}_4}$.

3.3.3 The Dirac Equation

In this section we carry out a full analysis of the scattering and emission of a charged probe of charge γ from the black hole. We would like to solve for the wavefunction of a probe of Poincare energy ϵ scattering off the background black hole. In [82], it was found that the ground state wavefunction describing a light BPS probe particle of charge γ in the background of another, heavy BPS particle of charge Γ, is given by a monopole

spherical harmonic [87] corresponding to a configuration with total angular momentum $(\langle\gamma,\Gamma\rangle - 1)/2$. This can be thought of as the light BPS probe going into a spin-1/2 state aligned with the radial magnetic field of the background BPS particle, thus minimizing the energy of the configuration, and contributing one spin quantum opposite to the intrinsic field angular momentum, which is $\langle\gamma,\Gamma\rangle/2$. This is analogous to the problem of scattering a Dirac particle of charge Ze in the background of a magnetic monopole of strength g [87,88], where the intersection product $\langle\gamma,\Gamma\rangle$ corresponds to the quantity Zeg. Since we are trying to solve the curved space version of this problem (though for higher energy states as well as the ground state), it is reasonable to assume that the wavefunction describing a probe particle emitted from the background black hole will obey the curved-space Dirac equation in the black hole background, and correspond to the probe going into a spin-1/2 state aligned with the radial magnetic field of the background black hole.

Using the vierbein formalism, the Dirac equation in curved space is:

$$i\gamma^a V_a^\mu \partial_\mu \Psi + \frac{i}{2}\gamma^a V_a^\mu V_b^\nu V_{c\nu;\mu}\Sigma^{bc}\Psi - \gamma^a V_a^\mu A_\mu \Psi = \mu\Psi, \tag{3.54}$$

where μ is the mass of the particle given by $\mu = |Z(\gamma, z)|$, A_μ is the electromagnetic gauge potential, and Ψ is a 4-component spinor. In our case A_μ is given by (3.25). Note that any choice of the vector potential A_ϕ around a magnetic monopole must have singularities. Thus, the specific form of A_ϕ given in (3.25) represents a gauge choice that is non-singular in some region R_a (in this case, the region $r > 0$, $0 \leq \phi < 2\pi$, and $0 \leq \theta < \pi$.) In order to cover the entire space outside the magnetic monopole, we must divide the space into two regions and use a different gauge in each region. We can define the second region R_b as

$r > 0$, $0 \leq \phi < 2\pi$, and $0 < \theta \leq \pi$, and use the gauge choice

$$A_\phi = -\frac{\langle \gamma, \Gamma \rangle}{2}(1 + \cos\theta) \tag{3.55}$$

in this region.

Because of this fact, the components of the Dirac spinor

$$\Psi = \begin{pmatrix} \psi_0 \\ \psi_1 \\ \psi_2 \\ \psi_3 \end{pmatrix}, \tag{3.56}$$

in a magnetic monopole background are given by sections on a line bundle, not a function [87]. The angular part of the section can be expanded in monopole spherical harmonics $Y_{j,l,m}(\theta, \phi)$ characterized by the quantum numbers (j, l, m), where

$$j = 0, \frac{1}{2}, 1, \ldots \tag{3.57}$$

$$l = |j|, |j| + 1, |j| + 2, \tag{3.58}$$

$$m = -l, -l + 1, \ldots, l, \tag{3.59}$$

and

$$Y_{j,l,m}(\theta, \phi) = e^{i((m+j)\phi}\Theta_{j,l,m}(\theta) \quad \text{in region } R_a \tag{3.60}$$

$$Y_{j,l,m}(\theta, \phi) = e^{i((m-j)\phi}\Theta_{j,l,m}(\theta) \quad \text{in region } R_b \tag{3.61}$$

for the same function $\Theta_{j,l,m}(\theta)$.

For a suitable choice of vierbeins (for details, see Appendix B.1), we substitute

the ansatz

$$\psi_0 = R_0(r)Y_{q+1/2,l,m}(\theta,\phi)e^{iq\phi}e^{-i\epsilon t} \tag{3.62}$$

$$\psi_1 = R_1(r)Y_{q-1/2,l,m}(\theta,\phi)e^{iq\phi}e^{-i\epsilon t} \tag{3.63}$$

$$\psi_2 = R_2(r)Y_{q+1/2,l,m}(\theta,\phi)e^{iq\phi}e^{-i\epsilon t} \tag{3.64}$$

$$\psi_3 = R_3(r)Y_{q-1/2,l,m}(\theta,\phi)e^{iq\phi}e^{-i\epsilon t} \tag{3.65}$$

into (3.54), where we have defined

$$q \equiv \frac{\langle \gamma, \Gamma \rangle}{2}. \tag{3.66}$$

In the case when $q > 0$, there is a possible solution with $\psi_0 = \psi_2 = 0$, and $l = q - \frac{1}{2}$. When $q < 0$, there is a possible solution with $\psi_1 = \psi_3 = 0$, and $l = -q - \frac{1}{2}$. As expected, these solutions correspond to the probe particle being aligned with the radial magnetic field of the background black hole. The two cases are exactly analogous so from now on we will assume that $q < 0$. We obtain coupled radial equations for $R_0(r)$ and $R_2(r)$ of the form:

$$e^{-U}(\partial_t + iA_t + i\mu)R_0 + \frac{e^{\frac{3U}{2}}}{r}\partial_r(re^{-\frac{U}{2}}R_2) = 0 \tag{3.67}$$

$$e^{-U}(\partial_t + iA_t - i\mu)R_2 + \frac{e^{\frac{3U}{2}}}{r}\partial_r(re^{-\frac{U}{2}}R_0) = 0. \tag{3.68}$$

3.3.4 The WKB Approximation

We cannot solve the radial part of the Dirac equation exactly in this background. So in order to compute the tunneling amplitude, we will solve for the radial components of the wavefunction using the WKB approximation.

In order to apply the WKB approximation, we first substitute $q \to q/\hbar$ and $\epsilon \to \epsilon/\hbar$. Using the ansatz (3.62) and defining $T_{0,2}(r) \equiv re^{-U/2}R_{0,2}(r)$ gives the following

equation for $T_0(r)$ (with an analogous equation for $T_2(r)$:

$$T_0'' = -\frac{e^{-4U}}{\hbar^2\left(1+\frac{c^2}{r^2}\right)}\left((\epsilon - A_t)^2 - e^{2U}\mu^2\right)T_0 \tag{3.69}$$

$$+ T_0' \frac{e^U\sqrt{1+c^2/r^2}}{(\epsilon e^{-U} - A_t e^{-U} + \mu)}\frac{d}{dr}\left[\frac{e^{-U}(\epsilon e^{-U} - A_t e^{-U} + \mu)}{\sqrt{1+c^2/r^2}}\right] \tag{3.70}$$

where a prime denotes differentiation with respect to r. Substituting the ansatz $T_{0,2} = B_{0,2}e^{iS_{0,2}/\hbar}$ and taking terms to leading order in $1/\hbar$, we find:

$$S_{0,2}'^2 = \frac{e^{-4U}}{\left(1+\frac{c^2}{r^2}\right)}\left((\epsilon - A_t)^2 - e^{2U}\mu^2\right). \tag{3.71}$$

Note that this is the same expression that gives the canonical momentum p_r in (3.49). We need to go to the next order in $1/\hbar$ to find the equation for $B_0(r)$ (an exactly analogous equation gives $B_2(r)$):

$$B_0 S_0'' + 2B_0' S_0' = \tag{3.72}$$

$$\left[\frac{\frac{d}{dr}(\epsilon e^{-U} - A_t e^{-U} + \mu)}{(\epsilon e^{-U} - A_t e^{-U} + \mu)} + e^U\sqrt{1+c^2/r^2}\frac{d}{dr}\left(\frac{e^{-U}}{\sqrt{1+c^2/r^2}}\right)\right]B_0 S_0' \tag{3.73}$$

This next order in the WKB approximation is necessary in order to derive the connection formulae needed to extend the solution past the classical turning points, where the WKB approximation becomes invalid. The connection formulae are derived in Appendix B.3. We can solve equations (3.71)-(3.72) in the region $r \lll \frac{1}{\tilde{c}_2}$ (recall that both turning points lie in this region for the class of background black holes we are considering), and then patch this solution to the WKB solution in the region $c \lll r$. The details of the calculation are given in Appendix B.2.

3.3.5 The Tunneling Amplitude

In the regime $c \lll \frac{1}{\tilde{c}_2} \sim \frac{1}{\tilde{c}_4}$ we find that

$$\cosh c_2, \cosh c_4 \approx 1 \tag{3.74}$$

$$\sinh c_2 \approx c\tilde{c}_2 \lll 1 \tag{3.75}$$

In order to calculate the tunneling amplitude for a probe particle, we want to find the equivalent of the probability density of the particle wavefunction at different values of r. In the case of a Dirac spinor, this is given by the time component of the conserved current density J^μ, which is given by:

$$J^\mu = \bar{\Psi}\underline{\gamma}^\mu\Psi, \tag{3.76}$$

$$\nabla_\mu J^\mu = 0, \tag{3.77}$$

where

$$\underline{\gamma}^\mu := V_a^\mu \gamma^a, \tag{3.78}$$

$$\bar{\Psi} := \Psi^\dagger\gamma^0, \tag{3.79}$$

and γ^0 indicates the flat-space gamma matrix.

For the background metric (3.18), J^0 is given by:

$$J^0 = e^{-U}(|R_0|^2 + |R_2|^2). \tag{3.80}$$

We now want to compute the ratio of charge densities at spatial infinity $r \to \infty$, and at the black hole horizon $r \to 0$. Given a conserved current J^μ satisfying $\nabla_\mu J^\mu = 0$, we can define the one-form $J_\mu = g_{\mu\nu}J^\nu$ and write the conservation condition as:

$$\mathrm{d}(\star J) = 0 \tag{3.81}$$

We then define the charge passing through a hypersurface $\mathcal{H}$ via:

$$Q_{\mathcal{H}} = -\int_{\mathcal{H}} \star J. \tag{3.82}$$

We take $\mathcal{H}$ to be a hypersurface of constant time, t. We can then write:

$$Q_{\mathcal{H}} = -\int_{\mathcal{H}} d^3x \sqrt{|h|} n_\mu J^\mu \tag{3.83}$$

where h_{ij} is the spatial metric and $n_\mu = g_{\mu\nu} n^\nu$ where n^ν is the normal vector to the hypersurface. We therefore have

$$n^\nu = (1, 0, 0, 0) \tag{3.84}$$

$$n_\mu = \left(-e^{2U}, 0, 0, 0\right) \tag{3.85}$$

$$\sqrt{|h|} = \sqrt{\frac{e^{-6U}}{(1 + c^2/r^2)} r^4 \sin^2\theta}. \tag{3.86}$$

We can then write:

$$Q_{\mathcal{H}} = \int_{\mathcal{H}} d^3x \sqrt{|h|}\, e^{2U}\, J^0 \tag{3.87}$$

$$= \int_{\mathcal{H}} dr\, d\theta\, d\phi\, e^U \sqrt{\frac{e^{-6U}}{(1 + c^2/r^2)} r^4 \sin^2\theta}\ (|R_0|^2 + |R_2|^2) \tag{3.88}$$

$$= \int_{\mathcal{H}} dr\, d\theta\, d\phi\, \frac{e^{-2U} r^2 \sin\theta}{\sqrt{1 + c^2/r^2}}\ (|R_0|^2 + |R_2|^2). \tag{3.89}$$

It follows that to get the charge density $q(r)$ at r, we should integrate just over θ, ϕ:

$$q(r) = \int_{\mathcal{H}} d\theta\, d\phi\, \frac{e^{-2U} r^2 \sin\theta}{\sqrt{1 + c^2/r^2}}\ (|R_0|^2 + |R_2|^2) \tag{3.90}$$

$$\sim \frac{e^{-2U} r^2}{\sqrt{1 + c^2/r^2}} (|R_0|^2 + |R_2|^2) \tag{3.91}$$

We can now calculate the charge densities at the black hole horizon, and at spatial infinity, using the form of the Dirac spinor found in Appendix B.2. We impose boundary

conditions so that the wavefunction is entirely outgoing at $r \to \infty$. In order to obtain the emission amplitude, we should compute the charge density at $r \to 0$ using only the outgoing component at the black hole horizon. We find that:

$$q(r)_{r\to\infty} = r^2(|R_0|^2 + |R_2|^2) = |\tilde{B}_0|^2 \tag{3.92}$$

$$q(r)_{r\to 0} = \frac{E_0 r}{c}(|R_0|^2 + |R_2|^2) = \frac{\alpha_0}{c^2(1-\beta\alpha_0)}|\tilde{B}_0|^2 \left(\Gamma_t - \frac{1}{2\Gamma_t}\right)^2 \tag{3.93}$$

for some constant $\tilde{B}_0$, where the tunneling rate Γ_t is given by (3.53). We can obtain the tunneling amplitude by taking the ratio of the charge densities:

$$\frac{q(r)_{r\to\infty}}{q(r)_{r\to 0}} = \frac{c^2(1-\beta\alpha_0)}{\alpha_0} \frac{1}{\left(\Gamma_t - \frac{1}{2\Gamma_t}\right)^2} \tag{3.94}$$

$$= \frac{c^2(1-\beta\alpha_0)}{\alpha_0} \frac{1}{\left(e^{-a_1\alpha_0\pi(\beta-1)} - \frac{1}{2}e^{a_1\alpha_0\pi(\beta-1)}\right)^2} \tag{3.95}$$

We can see that the tunneling amplitude depends on the parameter α_0, which is related to the difference between the gravitational and electrostatic parts of the static probe potential, as well as the energy of the probe (which is related to $(1-\beta\alpha_0)$). It also appears that the tunneling amplitude decreases to zero as the background black hole becomes extremal.

3.4 Discussion

We have initiated a study of the stability of a class of non-extremal black holes in $\mathcal{N} = 2$, $d = 4$ supergravity. Our results provide some clues as to how such a black hole perturbed away from extremality might evolve over time. If the black hole is BPS in the extremal limit, then for the range of parameters we have considered, then it can only emit probe particles γ such that the intersection product $\langle \gamma, \Gamma \rangle$ between the probe charge and

the black hole charge is zero. The static potential felt by such a probe is flat, so that there is no barrier to emission or absorption. Thus, we would expect that such a black hole would decay by the emission of these probes to spatial infinity until it became extremal.

If the black hole is non-BPS in the extremal limit, then it can emit probes of different charges. We found that the decay rate increases as the parameter α_0^2 decreases, where α_0^2 is related to the difference between the gravitational and electrostatic parts of the static probe potential. Thus, we expect probes with small α_0^2 to be emitted preferentially by the black hole. For the class of black holes we studied, we found that the probe potential has a single maximum at $r = r_0$, and decreases steadily as $r \to \infty$. Thus, as there is no local minimum in the probe potential, we expect that any particles emitted from the black hole will simply be ejected out to spatial infinity.

There are many possible routes for further investigation: it would be useful to extend these results to arbitrary values of the parameters $c, \frac{1}{\tilde{c}_2}$, and $\frac{1}{\tilde{c}_4}$, so that we are no longer restricted to the near-extremal limit. Another natural extension of our results would be to study the scattering of fermionic particles in the black hole background, and to compare the relative emission rates of different types of particles from the black hole.

Chapter 4

Tunneling between single and multi-centered black hole configurations

In this chapter we study the problem of finding a gravitational instanton that connects two vacuum states: one state corresponding to a single-centered extremal Reissner-Nordstrom (ERN) black hole configuration, and another state corresponding to a multi-centered ERN configuration. This instanton is interpreted as describing quantum tunneling between two different black hole solutions, analogous to the instanton for the symmetric double well. We evaluate the Euclidean action for this instanton and find that the amplitude for the tunneling process is equal to half the difference in entropy between the initial and final configurations.

In Section 4.1 we introduce the problem we are trying to solve and introduce

some motivation for working on the problem. In Section 4.2, we outline the background information necessary to understand the work in this Chapter. In Section 4.3 we present our results. In Section 4.3.1 we present the instanton solution corresponding to tunneling between single and multi-centered configurations, and describe its key features. In Section 4.3.2 we evaluate the Euclidean action for the instanton to find the tunneling amplitude. We conclude in Section 4.4.

4.1 Introduction

Instantons are solutions of the Euclidean equations of motion. As tunneling processes can be considered as propagation in Euclidean time, an instanton can describe tunneling transitions that are classically forbidden: for example, gravitational instantons, which are Riemannian solutions of the Einstein field equations, can describe changes in the topology of space [90]. In the semiclassical WKB approximation, the tunneling amplitude is given by the value of the Euclidean action for the instanton.

Gravitational instantons have been found that describe the pair production of Wheeler wormholes [91], and the fragmentation of a single charged $AdS_2 \times S_2$ universe into multiple, completely disconnected $AdS_2 \times S_2$ universes [92, 93]. But so far, an instanton has not been found that describes a transition between a single-centered black hole configuration to a *connected* multi-centered black hole configuration.

In this chapter we describe such an instanton, where the single-centered configuration is a charged Bertotti-Robinson (BR) universe (corresponding to the $AdS_2 \times S_2$ near-horizon region of an extremal Reissner-Nordstrom black hole) [95–97], as shown in

Figure 4.1, and the multi-centered configuration consists of a set of extremal Reissner-Nordstrom (ERN) black holes placed at arbitrary locations in an encapsulating BR universe, as shown in Figure 4.2 (the multi-centered configuration can also be interpreted as a single encapsulating $AdS_2 \times S_2$ throat that divides into multiple branches as we move deeper into the throat.) The total charge of the multi-centered solution is equal to the charge of the single-centered solution. Our instanton differs from the instanton describing the pair production of black holes [91], as it describes the splitting of an existing black hole throat. It also differs from the well-known Brill instanton [92] describing the fragmentation of a single $AdS_2 \times S_2$ throat into several completely disconnected $AdS_2 \times S_2$ throats. Brill's instanton describes vacuum tunneling between a single $AdS_2 \times S_2$ universe, and a set of multiple, disconnected, disjoint $AdS_2 \times S_2$ universes. Our instanton, on the other hand, describes vacuum tunneling between a single $AdS_2 \times S_2$ throat (corresponding to the black hole throat of a magnetically charged ERN black hole), and a branching $AdS_2 \times S_2$ throat (corresponding to the black hole throat of a magnetically charged ERN black hole that has split into several throats, the total charge of which is equal to the single throat configuration.) So the Brill instanton can be interpreted as describing the *fragmentation* of a single $AdS_2 \times S_2$ universe. Our instanton can be interpreted as describing the *splitting* of a single $AdS_2 \times S_2$ throat, which nevertheless remains in a single piece at spatial infinity. Thus, our instanton describes the splitting of an ERN black hole into multiple black holes, within the *same* universe: in contrast to the Brill instanton, which describes the fragmentation of one universe into several.

This instanton is analogous to the well-known instanton solution for the symmetric double well in one-dimensional quantum mechanics, as it connects two degenerate

vacua. Thus, rather than describing a decay process, this instanton describes quantum *mixing* between two vacuum states. The true ground state will therefore be a quantum superposition of all such configurations, where each configuration satisfies the condition that the sum of the charges of all the black holes is equal to the total charge of the single-centered configuration. Calculating the tunneling amplitude between the vacua, we find that it is equal to half the difference in entropy between the two configurations. This result agrees with the expectations of [94], where it was suggested that the splitting of ERN black holes could be exponentially suppressed by a tunneling amplitude proportional to the change in entropy before and after the splitting.

4.2 Background Information

In this section we introduce the background information on ERN black holes necessary to understand the material in this chapter.

4.2.1 The Black Hole Solutions

We begin by describing the black hole solutions corresponding to the two states connected by our instanton. These are solutions to the Einstein-Maxwell equations that describe magnetically charged black holes. In a spacetime with coordinates $(t, \vec{x})$, the metric and the electromagnetic field strengths are given by:

$$ds^2 = -H^{-2}dt^2 + H^2 d\vec{x}^2 \tag{4.1}$$

$$\star F = dt \wedge dH^{-1}, \tag{4.2}$$

where H is a harmonic function that satisfies

$$\nabla^2 H = 0, \tag{4.3}$$

where ∇^2 is the Laplacian on flat $\mathbb{R}^3$. This solution describes a Bertotti-Robinson (BR) type universe [95–97] containing a number of ERN black holes. The black holes may be located at arbitrary coordinate locations $\vec{x}_a$. If there are N black holes of charges $Q_1, \ldots, Q_N$, then the function H has the form:

$$H = \sum_{a=1}^{N} \frac{Q_a}{|\vec{x} - \vec{x}_a|}. \tag{4.4}$$

We denote the total charge by $Q_\infty \equiv Q_1 + \cdots + Q_N$. This solution has a tree-like geometry that is asymptotically $AdS_2 \times S_2$ at large radius, but then branches into smaller $AdS_2 \times S_2$ regions at the ERN black holes. The special case when $N = 1$ corresponds to a single-centered black hole solution, which is simply an $AdS_2 \times S_2$ space of charge $Q_\infty = Q_1$.

These solutions can also be derived by taking the limit $L_p \to 0$ (where L_p is the Planck length) of asymptotically flat multi-centered ERN black hole solutions with separations of order L_p^2 between the black holes [93]. As $L_p \to 0$, the asymptotically flat region decouples and we are left with an encapsulating throat of charge Q_∞ which splits into N throats of charge $Q_1, \ldots, Q_N$.

4.3 Results

4.3.1 The Gravitational Instanton

We want to consider a tunneling process in which a single-centered black hole configuration of charge Q_∞ splits into a multi-centered black hole configuration of charges

Figure 4.1 *The single-centered configuration, which is simply an $AdS_2 \times S_2$ Bertotti-Robinson universe with charge Q_∞.*

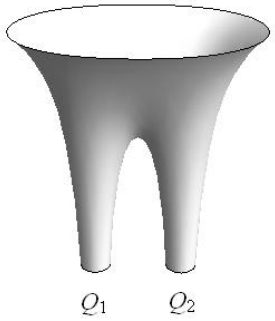

Figure 4.2 *A two-centered configuration, which consists of an encapsulating BR universe (i.e. an $AdS_2 \times S_2$ throat) containing two extremal Reissner-Nordstrom black holes of charge Q_1 and Q_2.*

$Q_1, \ldots, Q_N$ such that $Q_\infty = Q_1 + \cdots + Q_N$. This process should be described by a gravitational instanton, which is a solution to the Euclidean equations of motion. In order to describe a valid tunneling process [98], the Euclidean action of the instanton should be finite and real. Moreover, we should be able to define a Euclidean time coordinate τ such that slicing up the spacetime into hypersurfaces of constant τ takes us from an initial hypersurface Σ_i at $\tau = -\infty$ to a final hypersurface Σ_f at $\tau = \infty$. The induced metrics on Σ_i and Σ_f should be real, and correspond to spatial slices of the Lorentzian spacetimes that we want to connect via a tunneling trajectory (in this case, the single-centered and multi-centered solutions.) In order to allow the Euclidean solution to be joined smoothly to the Lorentzian solutions across Σ_i and Σ_f, the extrinsic curvature K_{ij} should vanish on both surfaces.

Our instanton satisfies all of these conditions. As mentioned in Section 4.1, our instanton differs from previously discovered instantons connecting single-centered to multi-centered black hole configurations as our instanton connects a single-centered configuration to a *connected* multi-centered configuration, rather than several completely disconnected spaces. In addition to this fundamental difference, there are also differences between in the explicit technical construction of the instanton. Brill's instanton has a limitation, in that Brill does not define initial and final surfaces that can be connected to Lorentzian spacetimes. Instead he merely defines "asymptotic regions" at past infinity and future infinity for Euclidean time, that approach the single $AdS_2 \times S_2$ throat and multiple disconnected $AdS_2 \times S_2$ throats respectively. However, it is not then clear how these asymptotic regions can join smoothly onto spacelike hypersurfaces of a Lorentzian spacetime. Maldacena, Michelson, and Strominger (MMS) [93] attempted to remedy this situation by defining

an instanton using different coordinates, with initial and final surfaces of zero extrinsic curvature that corresponded to spacelike slices of a single AdS space, and multiple disconnected AdS spaces respectively. However, this result still had several differences from our work. Firstly, of course, the final surface of the MMS instanton corresponds to completely disconnected $AdS_2 \times S_2$ universes, unlike our work where the multiple $AdS_2 \times S_2$ throats remain connected at the "top" of the throat. Secondly, the initial and final surfaces of the MMS instanton correspond to spatial slices of *global* $AdS_2 \times S_2$ spacetime, not Poincare $AdS_2 \times S_2$, as was the case with Brill, and as is the case in this work. This is an important distinction when it comes to interpreting the instanton as the splitting of the throat of an ERN black hole. Secondly, MMS assumed (but did not show) that the value of the Euclidean action for their instanton would be the same as the value Brill found. This might not necessarily be the case, given that MMS use a different set of coordinates from Brill.

We define initial and final surfaces for the instanton with zero extrinsic curvature. The initial surface is reached at $\tau = -\infty$ and the final surface at $\tau = \infty$, where τ is a suitably defined notion of Euclidean time. The initial surface is diffeomorphic to the spatial slice of a Lorentzian Poincare $AdS_2 \times S_2$ throat, and the final surface is diffeomorphic to the spatial slice of a Lorentzian spacetime that is the aforementioned Poincare $AdS_2 \times S_2$ space that splits into multiple $AdS_2 \times S_2$ spaces further down the throat, but remain joined at the "top" of the throat. It is important that we are considering Poincare rather than global $AdS_2 \times S_2$ space times, as we want to consider the splitting of black hole throats, and the throat of an ERN black hole is given by a Poincare AdS geometry.

Since we are dealing with Poincare $AdS_2 \times S_2$ throats at all times, the initial and final surfaces can be thought of as spatial slices through the black hole throats of two

different black hole configurations. The initial surface corresponds to a spatial slice through a single ERN black hole throat. The final surface corresponds to a spatial slice through the throat of an ERN black hole that has split into multiple ERN black holes further down the throat, but remain connected at the top of the original single throat so that the entire configuration looks like a single ERN black hole when viewed from far away.

In order to find the gravitational instanton, we first analytically continue the time coordinate to $w = -it$ to obtain a solution to the Euclidean equations of motion:

$$ds^2 = H^{-2}dw^2 + H^2 d\vec{x}^2 \tag{4.5}$$

$$\star F = -dw \wedge dH^{-1}, \tag{4.6}$$

We then define the coordinate [93]:

$$y = \left(\sum_{a=1}^{N} \frac{Q_a}{\sqrt{|\vec{x} - \vec{x}_a|}} \right)^2 \tag{4.7}$$

Finally, we can define the coodinates τ and σ (where in the end, we will take τ to be our Euclidean time coordinate):

$$\tau = \frac{1}{2} \log(w^2 + y^2) \tag{4.8}$$

$$\sigma = \arctan \frac{y}{w} \tag{4.9}$$

The relation between the coordinates (w, y) and (τ, σ) are shown in Figure 4.3, where the semicircles represent the hypersurfaces of constant τ, and σ is the angular coordinate. We let τ take the range of values $-\tau_0 < \tau < \tau_0$ for some τ_0, and we take σ to cover the range $\epsilon < \sigma < \pi/2$ for some infinitesimal $\epsilon > 0$. We have regulated the lower limit of σ as $\sigma = 0$ corresponds to spatial infinity. In the end we will first take the limit $\epsilon \to 0$, then $\tau_0 \to \infty$.

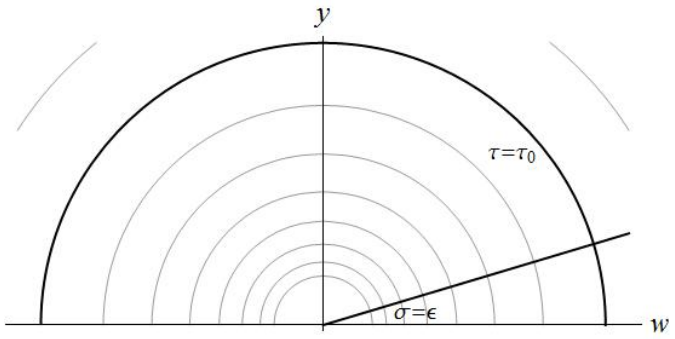

Figure 4.3 *The relationship between the coordinates (w, y) and (τ, σ). The semi-circles represent hypersurfaces of constant τ, and σ is the angular coordinate.*

We can now define the initial and final surfaces of the instanton. The initial surface Σ_i is the hypersurface with $\tau = -\tau_0$ and $\epsilon < \sigma < \pi/2$, and the final surface Σ_f is the hypersurface with $\tau = \tau_0$ and $\epsilon < \sigma < \pi/2$. We now have to show that the induced metric on these surfaces corresponds to spatial slices of the desired initial and final black hole configurations as we take the limit $\epsilon \to 0$, $\tau_0 \to \infty$, and that the extrinsic curvatures on these surfaces is zero.

On the initial surface Σ_i, we have $w^2 + y^2 \to 0$ as $\tau_0 \to \infty$. So we have

$$y \to \frac{Q_\infty^2}{|\vec{x}|} \tag{4.10}$$

And the metric (4.5) becomes:

$$ds^2 = Q_\infty^2 \left(\frac{dw^2 + dy^2}{y^2} + d\Omega^2 \right) \tag{4.11}$$

$$= Q_\infty^2 \left(\frac{d\sigma^2}{\sin^2 \sigma} + d\Omega^2 \right) \tag{4.12}$$

Explicit computation shows that the extrinsic curvature on this surface is zero. We can glue this to a spatial slice of Euclidean Poincare $AdS_2 \times S_2$ with charge Q_∞ [74], which is

the initial spacetime we want, by applying the coordinate transformation:

$$Y = \frac{2e^{\tau_0}\sin\sigma}{\cos\sigma + \cosh(\tau+\tau_0)} \tag{4.13}$$

$$W = \frac{2e^{\tau_0}\sinh(\tau+\tau_0)}{\cos\sigma + \cosh(\tau+\tau_0)} \tag{4.14}$$

The metric on Σ_i, where $W = 0$, in these coordinates is:

$$ds^2 = Q_\infty^2\left(\frac{dY^2}{Y^2} + d\Omega^2\right) \tag{4.15}$$

The coordinate Y covers the range $\epsilon e^{\tau_0} < Y < e^{\tau_0}$. If we first take the cutoff $\epsilon \to 0$, then take the limit $\tau_0 \to \infty$, this covers the entire $AdS_2 \times S_2$ space. We can therefore join Σ_i smoothly onto a spatial slice of a Lorentzian single-centered $AdS_2 \times S_2$ solution with charge Q_∞.

The final surface Σ_f is slightly more complicated. We first choose a cutoff $y = y_0$ for the y-coordinate. Then for the range of coordinates $y < y_0 + \delta$ on Σ_f for some fixed, small δ, we define the coordinates:

$$Y = y \tag{4.16}$$

$$W = w$$

This section of Σ_f corresponds to the blue segment of the hypersurface in Figure 4.4. For fixed y_0, as $\tau_0 \to \infty$, we find that $dw \to 0$ in this region. Specifically, the time-component of the metric is $H^{-2}dw^2$, and we have:

$$H^{-1}dw \to H^{-1}(e^\tau d\tau - e^\tau \sin\sigma d\sigma) \tag{4.17}$$

$$\to -y_0 H^{-1} d\sigma = O(e^{-\tau_0}) \tag{4.18}$$

$$\to 0 \tag{4.19}$$

as $\tau_0 \to \infty$, for $y < y_0 + \delta$. Thus the metric on this section of Σ_f is simply the Poincare spatial slice of the full multi-centered solution for the range of coordinates $\epsilon e^{\tau_0} < y < y_0 + \delta$. Explicit computation shows that the extrinsic curvature on this section vanishes.

For the range of coordinates $y > y_0 - \delta$ (corresponding to the red segment of the hypersurface in Figure 4.4), if we choose a large enough cutoff $y = y_0$, then we are on one of the throats of the multi-centered solution, as we are in the region of large y. Thus we have

$$y \to \frac{Q_a^2}{|\vec{x}|} \tag{4.20}$$

for one of the charges Q_a, where we have redefined the coordinate $\vec{x}$ so that the origin is centered at Q_a. The metric approaches

$$ds^2 = Q_a^2 \left(\frac{dw^2 + dy^2}{y^2} + d\Omega^2 \right) \tag{4.21}$$

$$= Q_a^2 \left(\frac{d\sigma^2}{\sin^2 \sigma} + d\Omega^2 \right) \tag{4.22}$$

as $y_0 \to \infty$. Explicit computation shows that the extrinsic curvature vanishes on this section of Σ_f. In this region, we apply the coordinate transformation:

$$Y = \frac{2e^{\tau} \sin \sigma}{\cos \sigma + \cosh(\tau - \tau_0)} \tag{4.23}$$

$$W = \frac{2e^{\tau} \sinh(\tau - \tau_0)}{\cos \sigma + \cosh(\tau - \tau_0)}$$

Note that in the overlap region, $y_0 - \delta < y < y_0 + \delta$, the definitions of the two sets of coordinates (4.16) and (4.23) agree in the limit $\tau_0 \to \infty$ for any fixed cutoff y_0.

The metric on this segment $y > y_0 - \delta$ of Σ_f is, for each throat:

$$ds^2 = Q_a^2 \left(\frac{dY^2}{Y^2} + d\Omega^2 \right) \tag{4.24}$$

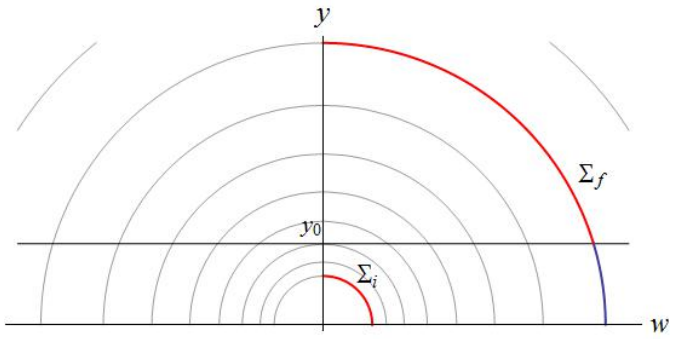

Figure 4.4 *The initial and final surfaces of the gravitational instanton. The initial surface Σ_i is given by the hypersurface $\tau = -\tau_0$, and the final surface Σ_f is given by the hypersurface $\tau = \tau_0$. In order to define the coordinate transformation that allows Σ_f to be glued to a spatial slice of the multi-centered solution, we define two regions on Σ_f: the blue region corresponds to $y < y_0 + \delta$, and the red region corresponds to $y > y_0 - \delta$, for some small fixed δ.*

This is the Poincare spatial slice of an $AdS_2 \times S_2$ throat of charge Q_a.

Thus, we find that the blue segment of Σ_f (corresponding to $y < y_0 + \delta$), can be glued to a spatial slice of a multi-centered solution cut off at $y = y_0$, while the red segment of Σ_f (corresponding to $y > y_0 + \delta$) consists of the spatial slices of multiple $AdS_2 \times S_2$ throats attached to the multi-centered solution at the cutoff. Note that the cutoff y_0 may be taken to be arbitrarily large. As with the initial surface Σ_i, the coordinate Y covers the range $\epsilon e^{\tau_0} < Y < e^{\tau_0}$. If we first take $\epsilon \to 0$, then take $\tau_0 \to \infty$, this covers the entire multi-centered solution. So Σ_f may be glued to the spatial slice of a multi-centered solution.

4.3.2 The Value of the Euclidean Action

We can now evaluate the Euclidean action for the instanton. The action is given by [73]:

$$-16\pi I = \int (R - F_{\mu\nu}F^{\mu\nu})\sqrt{g}d^4x + 2\int K\sqrt{h}d^3x + C[h_{ij}] \tag{4.25}$$

where h_{ij} is the induced metric on the boundary, K is the trace of the second fundamental form of the boundary, and $C[h_{ij}]$ is a term that depends solely on the induced metric at the boundary. The action can be converted into a pure boundary term [92]:

$$-8\pi I = \int (K + C_\mu \star F^{\mu\nu}n_\nu)\sqrt{h}d^3x + C[h_{ij}] \tag{4.26}$$

where C_μ is a vector potential defined by:

$$\star F = dC. \tag{4.27}$$

The spacetime is bounded by the following surfaces: the constant τ hypersurfaces $\tau = \pm\tau_0$, $\epsilon < \sigma < \pi/2$, the constant σ hypersurface $\sigma = \pi/2$, $-\tau_0 < \tau < \tau_0$, and the constant σ hypersurface $\sigma = \epsilon$, $-\tau_0 < \tau < \tau_0$.

On the first three hypersurfaces $\tau = \pm\tau_0$, $\epsilon < \sigma < \pi/2$ and $\sigma = \pi/2$, $-\tau_0 < \tau < \tau_0$, both the extrinsic curvature term and the electromagnetic term in (4.26) vanish, and thus do not contribute to the Euclidean action. The constant σ hypersurface $\sigma = \epsilon$, $-\tau_0 < \tau < \tau_0$ corresponds to the hypersurface $|\vec{x}| = e^{-\tau_0}/\epsilon$, $e^{-\tau_0} < w < e^{\tau_0}$. On this surface, we find that

$$K = \frac{1}{Q_\infty} \tag{4.28}$$

$$C_\mu \star F^{\mu\nu}n_\nu = -\frac{1}{Q_\infty}, \tag{4.29}$$

as $\epsilon \to 0$, so the two terms cancel, and this hypersurface also does not contribute to the Euclidean action.

Thus the only non-zero contributions to the Euclidean action come from the "edges" of the spacetime, at $\tau = \pm\tau_0$, $\sigma = \epsilon$, and $\tau = \pm\tau_0$, $\sigma = \pi/2$. The contribution from the "edges" can be calculated using the results in [99]: the contribution from an edge formed by two boundaries with spacelike normals n_0, n_1 (which is the case here, in Euclidean spacetime) is given by:

$$\int_{edge} -i\eta\sigma^{1/2} d^2x = -i\eta A_a \tag{4.30}$$

A_a is the area of the edge $|\vec{x} - \vec{x}_a| \to 0$, which is $4\pi Q_a^2$. The factor of $-i$ comes from Wick-rotation, and we have defined

$$\eta \equiv \text{arccosh}(-n_0 \cdot n_1) \tag{4.31}$$

In this case we have:

$$\text{arccosh}(-n_0 \cdot n_1) \to \text{arccosh}\,(0) \tag{4.32}$$

at all the edges. Note that the directions of the normals (i.e. whether they are inward or outward-pointing) does not matter, since we can take the branch of arccosh such that

$$\text{arccosh}\,(0) = \frac{i\pi}{2} \tag{4.33}$$

whether 0 is approached from above or below. Thus each edge will give a contribution of the same sign.

As with the contribution from the mantle surfaces, we want to normalize the Euclidean action so that it is zero when evaluated on a single-centered solution of total

charge $Q_\infty = Q_1$. Without normalizing, the edge terms for such a solution add up to:

$$\frac{1}{8\pi}(\frac{\pi}{2}A_1 + \frac{3\pi}{2}A_\infty) = \frac{1}{4}A_\infty, \tag{4.34}$$

where the first term comes from the edge $\tau = \tau_0$, $\sigma = \pi/2$, and the second term comes from the edges $\tau = -\tau_0$, $\sigma = \pi/2$, and $\tau = \pm\tau_0$, $\sigma = \epsilon$. So we must subtract $\frac{1}{4}A_\infty$ to obtain the correct normalization (this can be done by setting $C[h_{ij}] = -\frac{1}{4}A_\infty$.) This means that the total contribution from the edge terms is:

$$-\frac{1}{8\pi}\left(\sum_{a=1}^{N}\frac{\pi}{2}A_a + \frac{3\pi}{2}A_\infty - 2\pi A_\infty\right) = -\frac{1}{16}\sum_{a=1}^{N}A_a + \frac{1}{16}A_\infty \tag{4.35}$$

$$= \frac{\pi}{4}\left(Q_\infty^2 - \sum_{a=1}^{N}Q_a^2\right) \tag{4.36}$$

This is equal to half the difference in entropy between the initial and final configurations. This is different from the value of the Euclidean action for Brill's instanton, which is equal to the exact difference in entropy between a single $AdS_2 \times S_2$ throat and multiple completely disconnected $AdS_2 \times S_2$ throats. In some sense, it can be seen as natural that the probability amplitude for our instanton is half that for the Brill instanton, as the instanton in this work, unlike Brill's, connects a single $AdS_2 \times S_2$ throat to a configuration that branches into several $AdS_2 \times S_2$ throats at the bottom of the single throat, but remains connected at the top. Therefore, it can be said in some sense that only "half" of the original space becomes disconnected in the transition represented by the instanton, so that the corresponding tunneling amplitude is also half that of the process which gives a set of completely disconnected spacetimes.

4.4 Discussion

We have found an instanton that can be interpreted as a tunneling process between a single-centered black hole solution of charge Q_∞ to a multi-centered black hole solution of charges $Q_1, \ldots, Q_N$ such that $Q_\infty = Q_1 + \cdots + Q_N$. The amplitude for the tunneling process is equal to half the difference in entropy between the initial and final configurations. The black holes that we are considering are contained within an encapsulating $AdS_2 \times S_2$ throat. Thus we may consider them as black holes in a BR universe, or alternatively, as an $AdS_2 \times S_2$ throat that divides into multiple branches as we move deeper into the throat. In the latter interpretation, our instanton describes the splitting of the throat of an ERN black hole by quantum tunneling.

Ultimately, it would be desirable to find an instanton that describes the complete splitting of an ERN black hole into two or more ERN black holes separated by finite coordinate distances in an asymptotically flat space. Our instanton suggests that this process is not forbidden, as there is at least a finite probability for the throat of an ERN black hole to split into multiple throats.

Appendix A

Appendix to Chapter 2

A.1 Determining the Eigenvalues of the Angular Equation

We can obtain numerical values for the eigenvalue K of equation (2.20) by expanding the solutions $S(x)$ in a power series about $x = x_2$, and then enforcing the Z_2 symmetry boundary condition (i.e. the Neumann boundary condition) at $x = 0$, term by term in the power series, so that each additional term gives greater accuracy. To carry out this procedure, note that we can write the equation of motion for $S(x)$ as:

$$G(x)^2 S''(x) + G(x)G'(x)S'(x) + \left(G(x)(K + 2\mu A x) - \frac{\hat{m}^2}{\beta^2} \right) S(x) = 0 \tag{A.1}$$

Defining the polynomials:

$$s(x) \equiv G(x)^2 \tag{A.2}$$

$$t(x) \equiv G'(x)G(x) \tag{A.3}$$

$$u(x) \equiv G(x)(K + 2\mu A x) - \frac{\hat{m}^2}{\beta^2} \tag{A.4}$$

we can expand these as *finite* sums in powers of x, around $x = x_2$, so that $s(x) = \sum_{n=0}^{N} s_n (x - x_2)^n$, for example.

By Frobenius' method, the two linearly independent solutions to the above differential equation can be expanded about any regular, or regular singular point, as power series of the form:

$$S^{(1)}(x) = (x - x_2)^{\gamma_1} \sum_n b_n^{(1)} (x - x_2)^n \tag{A.5}$$

$$S^{(2)}(x) = (x - x_2)^{\gamma_2} \sum_n b_n^{(2)} (x - x_2)^n \tag{A.6}$$

as long as the difference between the two indices γ_1, γ_2 is not an integer. If the difference is an integer, then the two linearly independent solutions are of the form:

$$S^{(1)}(x) = (x - x_2)^{\gamma_1} \sum_n b_n^{(1)} (x - x_2)^n \tag{A.7}$$

$$S^{(2)}(x) = \log(x - x_2) + (x - x_2)^{\gamma_2} \sum_n b_n^{(2)} (x - x_2)^n \tag{A.8}$$

Writing $S(x) = (x - x_2)^{\gamma} \sum_n b_n (x - x_2)^n$, we see from substituting this into the equation of motion for $S(x)$ at lowest order that $\gamma_1 = \hat{m}/2$ and $\gamma_2 = -\hat{m}/2$. Thus the difference between γ_1 and γ_2 is always an integeter. In order to ensure regularity of $S(x)$ at $x = x_2$, we take $S(x) = (x - x_2)^{\gamma_1} \sum_n b_n^{(1)} (x - x_2)^n$. Inserting the finite partial sum into the equation of motion gives the b_n in terms of the recursion relation:

$$b_n = -\frac{1}{P_n} \sum_{k=0}^{n-1} \left(s_{n-k} k(k-1) + t_{n-k} k + u_{n-k} \right) b_k \tag{A.9}$$

$$P_n = n(n-1)s_0 + n t_0 + u_0, \tag{A.10}$$

where b_0 is a free parameter. Setting $b_0 = 1$, we then solve for the Z_2 symmetric boundary condition given by $S'(x = 0) = 0$ at the brane $x = 0$, imposed on the partial sum $S(x) =$

$(x-x_2)^\gamma \sum_{n=0}^{N} b_n (x-x_2)^n$ for some N. This constraint allows us to solve for K, given a pre-determined angular quantum number $\hat{m}$. As N is taken larger and larger, $S(x)$ is more closely approximated by the partial sum and K is given to greater levels of accuracy.

A.2 Determining the Eigenvalues of the Radial Equation

We follow the same procedure as in Appendix A.1 in order to solve the differential equation given in (2.25):

$$H(y)\Psi''(y) + \left(H'(y) + \frac{2i\hat{\omega}}{A\beta}\right)\Psi'(y) + (K - 2\mu A y)\Psi = 0 \tag{A.11}$$

This time we define

$$s(y) \equiv H(y) \tag{A.12}$$

$$t(y) \equiv H'(y) + \frac{2i\hat{\omega}}{A\beta} \tag{A.13}$$

$$u(y) \equiv K - 2\mu A y, \tag{A.14}$$

and we expand about $y = y_h$. Using the Frobenius method around this point, we find that $\Psi(y) = (y-y_h)^\gamma \sum_n a_n (y-y_h)^n$, where $\gamma = 0, -\frac{2i\hat{\omega}}{H'(y_h)}$. We found in Section 2.2.1 that these values of γ correspond exactly to ingoing and outgoing modes, respectively. Thus we take $\gamma = 0$ in order to impose the ingoing mode boundary condition at the black hole horizon. We find the following recursion relation for the a_n:

$$a_n = -\frac{1}{P_n}\sum_{k=0}^{n-1}\left(s_{n-k}k(k-1) + t_{n-k}k + u_{n-k}\right)a_k \tag{A.15}$$

$$P_n = n(n-1)s_0 + nt_0 + u_0, \tag{A.16}$$

We can determine the s_k, t_k, u_k numerically given the parameters μ, A, λ, and we have calculated K in the previous section. Thus the only unknown remaining is $\hat{\omega}$. We can therefore find $\Psi(y)$ as a partial sum, and then solve for $\hat{\omega}$ by imposing either the Dirichlet boundary condition at $y = 0$ or the Neumann boundary condition (which gives Z_2 symmetry) at $y = 0$. Note that we always find $\omega_I < 0$, which ensures that all the quasinormal modes are decaying and thus stable.

A.3 The Equations of Motion in Canonical Heun Form

Before we proceed with the calculations of the QNM for the conformal scalar field ϕ, it is enlightening to present the equations of motion in canonical form [**?**]. The analysis of the radial equation can be applied to the angular equation to show that it, too, has four regular singular points: two on the real line (one at the single real positive root of $G(x)$, the other at infinity), and two in the complex plane. Thus the solutions of both equations are Heun functions. A canonical differential equation of the Heun type takes the form:

$$Y''(y) + \left(\frac{\gamma}{y} + \frac{\delta}{y-1} + \frac{\epsilon}{y-a}\right) Y'(y) + \frac{\alpha\beta y - q}{y(y-1)(y-a)} Y = 0 \tag{A.17}$$

The Riemann P-symbol for a Heun equation of canonical form as shown in (A.17) is:

$$P = \begin{bmatrix} 0 & 1 & a & \infty & & \\ 0 & 0 & 0 & \alpha & y & q \\ 1-\gamma & 1-\delta & 1-\epsilon & \beta & & \end{bmatrix}, \tag{A.18}$$

In its most general form, a differential equation with four regular singular points, three in the finite complex plane at $y = y_0, y_1, y_2$, and one at infinity, can be written as:

$$Y''(y) + P(y)Y'(y) + Q(y)Y(y) = 0 \tag{A.19}$$

with the functions $P(y)$ and $Q(y)$ taking the form:

$$P(y) = \sum_{r=0}^{2} \frac{1 - \alpha_r - \alpha'_r}{y - y_r} \tag{A.20}$$

$$Q(y) = \frac{1}{H(y)} \left(q' + bb'y + \sum_{r=0}^{2} \frac{\alpha_r \alpha'_r H'(y_r)}{y - y_r} \right) \tag{A.21}$$

The solution to this equation is represnted by the Riemann P-symbol:

$$P = \begin{bmatrix} y_1 & y_2 & y_0 & \infty & & \\ \alpha_1 & \alpha_2 & \alpha_3 & b & y & q' \\ \alpha'_1 & \alpha'_2 & \alpha'_3 & b' & & \end{bmatrix}, \tag{A.22}$$

which is constrained by $b + b' + \sum_r \alpha_r + \alpha'_r = 2$. Our radial equation of motion takes the form:

$$R''(y) + \frac{H'(y)}{H(y)} R(y) + \frac{1}{H(y)} \left[K - 2\mu A y + \frac{\hat{\omega}^2}{A^2 \beta^2 H(y)} \right] = 0 \tag{A.23}$$

where we have defined β by setting $\Delta\phi = 2\pi\beta = 4\pi/|G'(x_2)|$ in order to compare the metric on the brane with the BTZ metric. We rescale ω as well as m because we need to rescale both the time coordinate t and the angular coordinate ϕ in order to compare to the BTZ metric.

We will now try to bring this to canonical Heun form. First we make the coordinate transformation:

$$\bar{y} = \frac{y - y_0}{y_1 - y_0} \tag{A.24}$$

With this variable, the equation of motion becomes:

$$\ddot{R}(y) + \frac{\dot{H}(\bar{y})}{H(\bar{y})} \dot{R}(y) + \frac{1}{\tilde{a} H(\bar{y})} \left[K - 2\mu A(y_0 + \tilde{a}\bar{y}) + \frac{\hat{\omega}^2}{A^2 \beta^2 \tilde{a}^3 H(\bar{y})} \right] R = 0 \tag{A.25}$$

where $H(\bar{y}) = \bar{y}(\bar{y}-1)(\bar{y}-a)$ and $\tilde{a} \equiv y_1 - y_0$. The locations of the finite regular singular points move to $0, 1$, and a, where

$$a \equiv \frac{y_2 - y_0}{y_1 - y_0}. \tag{A.26}$$

For the particular form of our radial equation, comparing the above equation to (A.20)-(A.21) and using the constraint $b + b' + \sum_r \alpha_r + \alpha'_r = 2$, it is straightforward to calculate that:

$$\alpha_r + \alpha'_r = 0 \tag{A.27}$$

$$bb' = -2\mu A \tag{A.28}$$

$$b' = 2 - b \tag{A.29}$$

$$q' = \frac{K - 2\mu A y_0}{y_1 - y_0} \tag{A.30}$$

The parameters in the Riemann P-symbol remain unchanged under this transformation, except of course for the argument y. Then, changing the independent variable according to

$$Y(y) \equiv y^{\alpha_1}(y-1)^{\alpha_2}(y-a)^{\alpha_3}\tilde{Y}(y) \tag{A.31}$$

transforms the Riemann P-symbol into the form:

$$P = \left[\begin{array}{cccccc} 0 & 1 & a & \infty & & \\ 0 & 0 & 0 & \alpha & y & q \\ -2\alpha_1 & -2\alpha_2 & -2\alpha_3 & \beta & & \end{array}\right] \tag{A.32}$$

where α, β, and q can be computed in terms of the parameters in the original form of the equation. The equation is thus converted into canonical Heun form. For the particular

form of our radial equation, it is straightforward to calculate that:

$$\alpha_1 = \frac{i\hat{\omega}}{aA\beta(y_1 - y_0)^2} \tag{A.33}$$

$$\alpha_2 = \frac{a}{a-1}\alpha_1 \tag{A.34}$$

$$\alpha_3 = \frac{1}{a-1}\alpha_1 \tag{A.35}$$

$$q = \frac{K - 2\mu A y_0}{y_1 - y_0} + 2a\alpha_2(1 + 2\alpha_1) \tag{A.36}$$

$$\alpha = b + 2\alpha_2 \tag{A.37}$$

$$\beta = b' + 2\alpha_2 \tag{A.38}$$

A similar procedure can also be carried out for the angular equation of motion. Note that I have defined q slightly differently from in Oscar and Maria's notes, so that my q is in fact their $q\alpha\beta$. Our results are the same except for a couple of numerical factors where I think there has just been a simple error in calculation. For instance their value of α_1 has an extra factor of $1/2$ relative to mine, and their value for $q\alpha\beta$ as given in Eq. (24) has an extra factor of $1/\mu A$ in the first term in the parentheses, and the second term has a factor y_1 in the numerator whereas I have y_0. I also do not have $\alpha = \beta = \delta$. The biggest difference is that I have $\alpha_1 \sim i\omega$ rather than $\alpha_1 \sim \omega$, which is a consequence of the ω^2 term in the differential equation having a positive sign, rather than a negative sign like the m^2 term in the angular equation.

A similar process can be carried out for the angular equation, where we find that

$$\alpha_r + \alpha_r' = 0 \tag{A.39}$$

$$bb' = -2\mu A \tag{A.40}$$

$$b' = 2 - b \tag{A.41}$$

$$q' = \frac{K - 2\mu A x_2}{x_1 - x_2} \tag{A.42}$$

For the original, untransformed equation, and that for the transformed equation:

$$\alpha_1 = \frac{\hat{m}}{a\beta(x_1 - x_2)^2} \tag{A.43}$$

$$\alpha_2 = \frac{a}{a-1}\alpha_1 \tag{A.44}$$

$$\alpha_3 = \frac{1}{a-1}\alpha_1 \tag{A.45}$$

$$q = \frac{K - 2\mu A x_2}{x_1 - x_2} + 2a\alpha_2(1 + 2\alpha_1) \tag{A.46}$$

$$\alpha = b + 2\alpha_2 \tag{A.47}$$

$$\beta = b' + 2\alpha_2 \tag{A.48}$$

Where this time we have $\alpha_1 \sim m$, not $\alpha_1 \sim im$.

Appendix B

Appendix to Chapter 3

B.1 The Dirac Equation in the Vierbein Formalism

Here we give the explicit form of the Dirac equation for a particular choice of vierbein. We use the following representation for the γ-matrices in the Dirac equation (3.54):

$$\gamma^0 = \begin{pmatrix} 1 & 0 \\ 0 & -1 \end{pmatrix} \qquad \gamma^i = \begin{pmatrix} 0 & -\sigma^i \\ \sigma^i & 0 \end{pmatrix} \tag{B.1}$$

and the following representation for Σ^{ab}:

$$\Sigma^{ab} = -\frac{1}{4}[\gamma^a, \gamma^b] \tag{B.2}$$

We use the following choice of vierbein:

$$V^0 = e^U\, dt \tag{B.3}$$

$$V^1 = e^{-U} r\, d\theta \tag{B.4}$$

$$V^2 = e^{-U} r \sin\theta\, d\phi \tag{B.5}$$

$$V^3 = e^{-U}\sqrt{1+\frac{c^2}{r^2}}\, dr \tag{B.6}$$

The Dirac equation for a spinor

$$\Psi = \begin{pmatrix} \psi_0 \\ \psi_1 \\ \psi_2 \\ \psi_3 \end{pmatrix} \tag{B.7}$$

then becomes:

$$e^{-U}(\partial_t + iA_t + i\mu)\psi_0 + \frac{e^{\frac{3U}{2}}}{r}\partial_r(re^{-\frac{U}{2}}\psi_2)\sqrt{1+\frac{c^2}{r^2}} \tag{B.8}$$

$$+\frac{e^U}{r}\left(\partial_\theta - \frac{i}{\sin\theta}\partial_\phi - \left(q-\frac{1}{2}\right)\cot\theta + \frac{q}{\sin\theta}\right)\psi_3 = 0 \tag{B.9}$$

$$e^{-U}(\partial_t + iA_t + i\mu)\psi_1 - \frac{e^{\frac{3U}{2}}}{r}\partial_r(re^{-\frac{U}{2}}\psi_3)\sqrt{1+\frac{c^2}{r^2}} \tag{B.10}$$

$$+\frac{e^U}{r}\left(\partial_\theta + \frac{i}{\sin\theta}\partial_\phi + \left(q+\frac{1}{2}\right)\cot\theta - \frac{q}{\sin\theta}\right)\psi_2 = 0 \tag{B.11}$$

$$e^{-U}(\partial_t + iA_t - i\mu)\psi_2 + \frac{e^{\frac{3U}{2}}}{r}\partial_r(re^{-\frac{U}{2}}\psi_0)\sqrt{1+\frac{c^2}{r^2}} \tag{B.12}$$

$$+\frac{e^U}{r}\left(\partial_\theta - \frac{i}{\sin\theta}\partial_\phi - \left(q-\frac{1}{2}\right)\cot\theta + \frac{q}{\sin\theta}\right)\psi_1 = 0 \tag{B.13}$$

$$e^{-U}(\partial_t + iA_t - i\mu)\psi_3 - \frac{e^{\frac{3U}{2}}}{r}\partial_r(re^{-\frac{U}{2}}\psi_1)\sqrt{1+\frac{c^2}{r^2}} \tag{B.14}$$

$$+\frac{e^U}{r}\left(\partial_\theta + \frac{i}{\sin\theta}\partial_\phi + \left(q+\frac{1}{2}\right)\cot\theta - \frac{q}{\sin\theta}\right)\psi_0 = 0 \tag{B.15}$$

where we have defined

$$q \equiv \frac{\langle \gamma, \Gamma \rangle}{2}. \tag{B.16}$$

We now use the fact that

$$\mathcal{D} \equiv -\partial_\theta - \frac{i}{\sin\theta}\partial_\phi + j\cot\theta \tag{B.17}$$

$$\bar{\mathcal{D}} \equiv -\partial_\theta + \frac{i}{\sin\theta}\partial_\phi - j\cot\theta \tag{B.18}$$

are raising and lowering operators for the monopole spherical harmonics that satisfy:

$$\mathcal{D}Y_{j,l,m} = \sqrt{(l-j)(l+j+1)}Y_{j+1,l,m} \tag{B.19}$$

$$\bar{\mathcal{D}}Y_{j,l,m} = -\sqrt{(l+j)(l-j+1)}Y_{j-1,l,m} \tag{B.20}$$

We substitute the ansatz:

$$\psi_0 = R_0(r)Y_{q+1/2,l,m}(\theta,\phi)e^{iq\phi}e^{-i\epsilon t} \tag{B.21}$$

$$\psi_1 = R_1(r)Y_{q-1/2,l,m}(\theta,\phi)e^{iq\phi}e^{-i\epsilon t} \tag{B.22}$$

$$\psi_2 = R_2(r)Y_{q+1/2,l,m}(\theta,\phi)e^{iq\phi}e^{-i\epsilon t} \tag{B.23}$$

$$\psi_3 = R_3(r)Y_{q-1/2,l,m}(\theta,\phi)e^{iq\phi}e^{-i\epsilon t}, \tag{B.24}$$

and see that if $q > 0$, then there is a possible set of solutions to the Dirac equation with $\psi_0 = \psi_2 = 0$, and $l = q - \frac{1}{2}$. Similarly, if $q < 0$, then there is a possible set of solutions with $\psi_1 = \psi_3 = 0$, and $l = -q - \frac{1}{2}$.

B.2 Solving the Dirac Equation Using the WKB Approximation

Here we give the details of the calculations for solving the Dirac Equation using the WKB approximation. As shown in Section 3.3.4, this comes down to solving equations (3.71) and (3.72) for the radial parts of the Dirac spinor components.

In the region $r \ggg c$, Eq. (3.71) becomes:

$$S_0'^2 = E_0 A_1^2 \alpha_0^2 \left(1 + \frac{E_0^{\frac{1}{2}}}{r}\right)^2 \tag{B.25}$$

and Eq. (3.72) becomes:

$$r\left(1 + \frac{r}{E_0^{1/2}}\right)\left(B_0 S_0'' + 2B_0' S_0'\right) + B_0 S_0' = 0 \tag{B.26}$$

These equations can be solved exactly to give:

$$B_0(r) = \tilde{B}_0 \tag{B.27}$$

$$S_0(r) = \pm \frac{a_1 \alpha_0}{E_0^{\frac{1}{2}}}(r + E_0^{\frac{1}{2}} \log r) \tag{B.28}$$

As $r \to \infty$, the solutions become:

$$\frac{e^{U/2}}{r} B_0(r) = \frac{\tilde{B}_0}{r} \tag{B.29}$$

$$S_\pm(r) = \pm \frac{a_1 \alpha_0}{E_0^{\frac{1}{2}}} r \tag{B.30}$$

Imposing outgoing boundary conditions at infinity (so we only keep S_+), the far region solution is:

$$\psi \sim \frac{\tilde{B}_0}{r} e^{i a_1 \alpha_0 E_0^{-\frac{1}{2}} r} \tag{B.31}$$

In order to patch the solutions in the regions $r \ggg c$ and $r \lll \frac{1}{\tilde{c}_2}$, we evaluate $B_0(r)$ and $S_+(r)$ in the limit $r \lll \frac{1}{\tilde{c}_2}$, which gives:

$$\frac{e^{U/2}}{r} B_0(r) = \frac{\tilde{B}_0}{r^{\frac{1}{2}} E_0^{\frac{1}{4}}} \tag{B.32}$$

$$S_+(r) = a_1 \alpha_0 \log r \tag{B.33}$$

Thus the solution in the region $r \ggg c$ is:

$$\psi \sim \frac{\tilde{B}_0}{r^{\frac{1}{2}} E_0^{\frac{1}{4}}} r^{i a_1 \alpha_0} \tag{B.34}$$

Defining $z \equiv \frac{r^2}{c^2}$, in the region $r \lll \frac{1}{\tilde{c}_2}$, Eq. (3.71) becomes:

$$S_0'^2 = \frac{a_1^2}{4z^2(1+z)} \left((\beta\alpha_0 - \sqrt{1+z})^2 + (\alpha_0^2 - 1) z \right), \tag{B.35}$$

where a prime denotes differentiation with respect to z. And Eq. (3.72) becomes:

$$2(1+z) B_0 (S_0' + 2z S_0'') \tag{B.36}$$

$$+ 2z \left[1 - 2(1+z) \left(\frac{z^{1/2} \frac{d}{dz} (z^{-1/2} (\beta\alpha_0 - \sqrt{1+z}))}{\beta\alpha_0 - \sqrt{1+z} - z^{1/2} \sqrt{1-\alpha_0^2}} \right) \right] B_0 S_0' \tag{B.37}$$

$$+ 8z(1+z) B_0' S_0' = 0 \tag{B.38}$$

Equation (B.35) can be solved exactly to give:

$$S_0(z) = S_\pm(z) \tag{B.39}$$

$$\begin{aligned} &= \pm \frac{a_1}{2} \Big[-2\beta\alpha_0 \text{Arctanh}(\sqrt{1+z}) - \log(-z) + 2\alpha_0 \log \left[-\beta + \alpha_0 \sqrt{1+z} + f(z) \right] \\ &+ (1 - \beta\alpha_0) \log \left[1 - f(z) + \alpha_0 \left(\alpha_0 (-1 + \sqrt{1+z}) + \beta^2 \alpha_0 - \beta (1 + \sqrt{1+z} - f(z)) \right) \right] \\ &+ (1 + \beta\alpha_0) \log \left[1 + f(z) + \alpha_0 \left(-\alpha_0 (1 + \sqrt{1+z}) + \beta^2 \alpha_0 + \beta (1 - \sqrt{1+z} + f(z)) \right) \right] \Big] \end{aligned} \tag{B.40}$$

where

$$f(z) \equiv \sqrt{1 - 2\beta\alpha_0\sqrt{1+z} + (z+\beta^2)\alpha_0^2}, \tag{B.41}$$

The form of $B_0(z)$ may also be determined exactly, but we will not give it here as it is extremely complicated and not particularly illuminating.

In order to patch the solution to the region $r \ggg c$, we solve Eq. (3.71)-(3.72) for $z \ggg 1$:

$$S_0'^2 = \frac{a_1^2\alpha_0^2}{4z^2} \tag{B.42}$$

$$4zB_0(S_0' + zS_0'') + 8z^2B_0'S_0' = 0 \tag{B.43}$$

to give:

$$\frac{e^{U/2}}{r}B_0(z) \sim \frac{1}{z^{\frac{1}{4}}} \tag{B.44}$$

$$S_\pm(z) = \pm\frac{a_1\alpha_0}{2}\log z \tag{B.45}$$

Matching to (B.34), we find that the solution in the region $z \ggg 1$ is:

$$\psi \sim \frac{\tilde{B}_0 c^{ia_1\alpha_0}}{E_0^{\frac{1}{4}} c^{\frac{1}{2}} z^{\frac{1}{4}}} z^{i\frac{a_1\alpha_0}{2}} \tag{B.46}$$

We can extend this solution up to the outer turning point at $z = z_+$, by taking $S_+(z)$ to select the wave that gives this form of ψ for $z \ggg 1$. At the turning point, the WKB approximation becomes invalid, as $B_0(z)$ diverges. Thus, in order to continue the WKB solution past z_+, we must derive connection formulas that allow us to patch together the solutions in the regions $z < z_-$ and $z > z_-$. We then repeat the procedure at the other turning point z_-. This can be done using Airy functions: detailed calculations are given in Appendix B.3.

Using the connection formulas, we find that the solution in the region $z < z_-$ is:

$$\psi \sim \frac{c^{ia_1\alpha_0}}{E_0^{\frac{1}{4}} c^{\frac{1}{2}}} B_0(z) \left(\left(\Gamma_t - \frac{1}{2\Gamma_t} \right) e^{iS_+(z)} - i \left(\Gamma_t + \frac{1}{2\Gamma_t} \right) e^{iS_-(z)} \right) \tag{B.47}$$

where the tunneling amplitude Γ_t is given by (3.53). The functions $B_0(z)$ and $S_\pm(z)$ in the region $z \lll 1$ are determined by the equations:

$$S_0'^2 = \frac{a_1^2}{4z^2}(1 - \beta\alpha_0)^2 \tag{B.48}$$

$$4B_0(S_0' + zS_0'') + 8zB_0'S_0' = 0, \tag{B.49}$$

which give:

$$B_0(z) = \frac{\alpha_0^{\frac{1}{2}}}{(1 - \beta\alpha_0)^{\frac{1}{2}}} \frac{c^{ia_1\alpha_0}}{E_0^{\frac{1}{4}} c^{\frac{1}{2}}} \tilde{B}_0 \tag{B.50}$$

$$S_0(z)_\pm = \pm \frac{a_1}{2}(1 - \beta\alpha_0) \log z \tag{B.51}$$

where $\tilde{B}_0$ is a constant. The wavefunction in the region $z \lll 1$ is thus:

$$\psi \sim \frac{e^{U/2}}{r} B_0 e^{iS_0/\hbar} \tag{B.52}$$

$$= \frac{\alpha_0^{\frac{1}{2}}}{(1 - \beta\alpha_0)^{\frac{1}{2}}} \frac{c^{ia_1\alpha_0}}{E_0^{\frac{1}{2}} c} \tilde{B}_0 z^{-1/4} \left(\left(\Gamma_t - \frac{1}{2\Gamma_t} \right) z^{+\frac{ia_1}{2}(1-\beta\alpha_0)} - i \left(\Gamma_t + \frac{1}{2\Gamma_t} \right) z^{-\frac{ia_1}{2}(1-\beta\alpha_0)} \right) \tag{B.53}$$

It may appear that the solution blows up and becomes unphysical as $z \to 0$, but as we will see in Section (3.3.5), this is not a problem as the charge density always remains finite. This solution is the limit of the general solution for $z \lll 1$.

B.3 Deriving the connection formulas for the WKB approximation using Airy functions

Here we outline the calculation for deriving the connection formulas that allow the WKB solutions to be extended across the turning points at z_+ and z_-. The general procedure is to solve radial equation using a linear approximation to the potential at the turning point, and then match this solution to the WKB approximation to the left and right of the turning point.

If we define the potential

$$V(z) \equiv \frac{a_1^2}{4z^2(1+z)}\left[\left(\beta\alpha_0 - \sqrt{1+z}\right)^2 + (\alpha_0^2 - 1)z\right], \tag{B.54}$$

then the radial equations for the WKB ansatz $\psi = B_r(r)e^{\frac{i}{\hbar}(S(r)+\epsilon t)}Y_{q,l,m}(\theta,\phi)$ are:

$$S'^2 = V(z) \tag{B.55}$$

$$2(1+z)B_r(S' + 2zS'') + 2z\left[1 - 2(1+z)\left(\frac{z^{1/2}\frac{d}{dz}(z^{-1/2}(\beta\alpha_0 - \sqrt{1+z}))}{\beta\alpha_0 - \sqrt{1+z} - z^{1/2}\sqrt{1-\alpha_0^2}}\right)\right]B_r S' \tag{B.56}$$

$$+ 8z(1+z)B_r' S' = 0 \tag{B.57}$$

We can rewrite the second equation as:

$$2(1+z)B_r(S' + 2zS'') + 8z(1+z)B_r' S' + 2z\left[1 - 2(1+z)M_1(z,\alpha_0,\beta)\right]B_r S' = 0 \tag{B.58}$$

for some function $M_1(z,\alpha_0,\beta)$.

The exact radial equation, given by (3.69), is:

$$T'' + M(z,\alpha_0,\beta)T' + V(z)T = 0 \tag{B.59}$$

for some function $M(z, \alpha_0, \beta)$, where $T(r) \equiv re^{-U/2}R(r)$ and $R(r)$ is the radial part of the Dirac spinor components.

The Linear Approximation

Consider a turning point at $z = z_0$. Defining the coordinate $w \equiv z - z_0$, we can take the linear approximation to the potential around z_0:

$$V(z) \approx V(z_0) + V'(z_0)w \tag{B.60}$$

$$= \rho w \tag{B.61}$$

where $\rho \equiv V'(z_0)$. Note that we have $\rho < 0$ for $z_0 = z_-$ and $\rho > 0$ for $z_0 = z_+$. The radial equation can then be approximated as:

$$T''(w) + M(z_0, \alpha_0, \beta)T'(w) + \rho w T(w) = 0 \tag{B.62}$$

This equation has the general solution:

$$T(w) = e^{\frac{-wM(z_0,\alpha_0,\beta)}{2}} \left[C_1 \mathrm{Ai}(w') + C_2 \mathrm{Bi}(w')\right] \tag{B.63}$$

where $\mathrm{Ai}(w')$ and $\mathrm{Bi}(w')$ are Airy functions, and we have defined

$$w' \equiv (-\rho)^{\frac{1}{3}} w + \frac{M(z_0, \alpha_0, \beta)^2}{4(-\rho)^{\frac{2}{3}}} \tag{B.64}$$

At each turning point we assume that there is a region in which the linear approximation is valid, and that the second term in the expression for w' is negligible compared to the first, so that we can take:

$$w' \approx (-\rho)^{\frac{1}{3}} w. \tag{B.65}$$

The turning point at z_+

First consider the turning point at $z = z_+$. The general solution in the region around z_+ where the linear approximation is valid, is:

$$e^{\frac{-wM(z_+,\alpha_0,\beta)}{2}}\left[\tilde{C}_1\mathrm{Ai}(w') + \tilde{C}_2\mathrm{Bi}(w')\right] \tag{B.66}$$

where w' is defined as in (B.65). Since ρ is positive, we find that

$$w' \sim (-1)^{\frac{1}{3}}\rho^{\frac{1}{3}}w, \tag{B.67}$$

and thus in order to match the above solutions to the WKB approximation to the left and right of z_+, we need the asymptotic behavior of the Airy functions for $w' \to (-1)^{\frac{1}{3}} \times -\infty$:

$$\mathrm{Ai}(w') \sim \frac{1}{2\sqrt{\pi}(-w')^{\frac{1}{4}}}\left[-ie^{\frac{2i}{3}(-w')^{3/2}} + e^{\frac{-2i}{3}(-w')^{3/2}}\right] \tag{B.68}$$

$$\mathrm{Bi}(w') \sim \frac{1}{2\sqrt{\pi}(-w')^{\frac{1}{4}}}\left[-ie^{\frac{-2i}{3}(-w')^{3/2}} + e^{\frac{2i}{3}(-w')^{3/2}}\right] \tag{B.69}$$

and $w' \to (-1)^{\frac{1}{3}} \times \infty$:

$$\mathrm{Ai}(w') \sim \frac{1}{2\sqrt{\pi}w'^{\frac{1}{4}}}e^{\frac{2}{3}w'^{3/2}} \tag{B.70}$$

$$\mathrm{Bi}(w') \sim \frac{1}{\sqrt{\pi}w'^{\frac{1}{4}}}\left[\frac{i}{2}e^{\frac{2}{3}w'^{3/2}} + e^{-\frac{2}{3}w'^{3/2}}\right] \tag{B.71}$$

We now need to solve the WKB equations to the left and right of the turning point. The radial equations for the WKB ansatz in the region where the linear approximation is valid are:

$$S'(w)^2 = \rho w \tag{B.72}$$

$$2(1+z_+)B_r(S' + 2z_+S'') + 8z_+(1+z_+)B_r'S' \tag{B.73}$$

$$+ 2z_+\left[1 - 2(1+z_+)M_1(z_+,\alpha_0,\beta)\right]B_rS' = 0 \tag{B.74}$$

These equations have the solutions:

$$S(w) = \pm\frac{2i}{3}\sqrt{\rho w^3} \tag{B.75}$$

and

$$B_r = \frac{B_0 e^{-\frac{wM(z_+,\alpha,\beta)}{2}}}{w^{\frac{1}{4}}}, \tag{B.76}$$

where B_0 is a constant and $M(z_+, \alpha, \beta)$ is the same function as in (B.86). Note that ρw^3 is negative on the left of the turning point, and positive on the right.

Since we are imposing the boundary condition that only the outgoing wave is present at spatial infinity, the WKB solution to the right of the turning point is:

$$\frac{B_0 e^{-\frac{wM(z_+,\alpha,\beta)}{2}}}{w^{\frac{1}{4}}} e^{\frac{2i}{3}\sqrt{\rho w^3}} \tag{B.77}$$

In order to match the linear solution in (B.66) to the WKB solution, note that:

$$\frac{2}{3}(w')^{\frac{3}{2}} = \frac{2i}{3}(\rho w^3)^{\frac{1}{2}} \tag{B.78}$$

and use the asymptotic form of the Airy functions as $w' \to (-1)^{\frac{1}{3}} \times \infty$. We assume that there is a region in which the linear approximation is valid, and $|w'|$ is large enough for the linear solution to be well approximated by this asymptotic form. We find that:

$$\tilde{C}_1 = 2\sqrt{\pi}(-1)^{\frac{1}{12}}\rho^{\frac{1}{12}}B_0 \tag{B.79}$$

$$\tilde{C}_2 = 0. \tag{B.80}$$

We now want to match the linear solution to the WKB solution on the left of the turning point. In this region, the general WKB solution is:

$$\frac{e^{-\frac{wM(z_+,\alpha,\beta)}{2}}}{w^{\frac{1}{4}}}\left[\tilde{D}_1 e^{-\frac{2\sqrt{\rho}}{3}w^{3/2}} + \tilde{D}_2 e^{\frac{2\sqrt{\rho}}{3}w^{3/2}}\right] \tag{B.81}$$

The linear solution takes the following asymptotic form as $w' \to (-1)^{\frac{1}{3}} \times -\infty$:

$$\frac{\tilde{C}_1 e^{-\frac{wM(z_0,\alpha,\beta)}{2}}}{2\sqrt{\pi}(-w')^{\frac{1}{4}}}\left[-ie^{\frac{2i}{3}(-w')^{3/2}} + e^{\frac{-2i}{3}(-w')^{3/2}}\right] \tag{B.82}$$

where

$$\frac{2}{3}(-w')^{\frac{3}{2}} = \frac{2i}{3}(\rho)^{\frac{1}{2}}(-w)^{\frac{3}{2}} \tag{B.83}$$

Matching the linear solution to the WKB solution to the left of the turning point gives:

$$\tilde{D}_1 = -i\tilde{D}_2 \tag{B.84}$$

$$= -ie^{-i\pi/4}B_0. \tag{B.85}$$

The turning point at z_-

We now repeat the derivation of the connection formulas at $z = z_-$. The general solution in the region around z_- where the linear approximation is valid is:

$$e^{\frac{-wM(z_-,\alpha_0,\beta)}{2}}\left[C_1\mathrm{Ai}(w') + C_2\mathrm{Bi}(w')\right], \tag{B.86}$$

As ρ is now negative, and $w' \sim (-\rho)^{\frac{1}{3}}w$, we need the asymptotic behavior of the Airy functions for $w' \to -\infty$:

$$\mathrm{Ai}(w') \sim \frac{1}{2i\sqrt{\pi}(-w')^{\frac{1}{4}}}\left[e^{\frac{i\pi}{4}}e^{\frac{2i}{3}(-w')^{3/2}} - e^{\frac{-i\pi}{4}}e^{\frac{-2i}{3}(-w')^{3/2}}\right] \tag{B.87}$$

$$\mathrm{Bi}(w') \sim \frac{1}{2\sqrt{\pi}(-w')^{\frac{1}{4}}}\left[e^{\frac{i\pi}{4}}e^{\frac{2i}{3}(-w')^{3/2}} + e^{\frac{-i\pi}{4}}e^{\frac{-2i}{3}(-w')^{3/2}}\right] \tag{B.88}$$

and for $w' \to \infty$:

$$\mathrm{Ai}(w') \sim \frac{1}{2\sqrt{\pi}w'^{\frac{1}{4}}}e^{-\frac{2}{3}w'^{3/2}} \tag{B.89}$$

$$\mathrm{Bi}(w') \sim \frac{1}{\sqrt{\pi}w'^{\frac{1}{4}}}e^{\frac{2}{3}w'^{3/2}} \tag{B.90}$$

The WKB solution to the right of the turning point is:

$$\frac{e^{-\frac{wM(z_-,\alpha,\beta)}{2}}}{w^{\frac{1}{4}}}\left[D_1 e^{\frac{2\sqrt{|\rho|}}{3}w^{3/2}} + D_2 e^{-\frac{2\sqrt{|\rho|}}{3}w^{3/2}}\right] \tag{B.91}$$

where D_1 and D_2 are related to $\tilde{D}_1$ and $\tilde{D}_2$ in (B.84) by:

$$\tilde{D}_1 = \Gamma_{\mathrm{t}} D_1 \tag{B.92}$$

$$\tilde{D}_2 = \frac{1}{\Gamma_{\mathrm{t}}} D_2 \tag{B.93}$$

$$\Gamma_{\mathrm{t}} \equiv e^{-\int_{z_-}^{z_+} |R'(z')| dz'} \tag{B.94}$$

On the left hand side of the turning point, the general WKB solution is:

$$\frac{e^{-\frac{wM(z_0,\alpha,\beta)}{2}}}{w^{\frac{1}{4}}}\left[G_1 e^{-\frac{2i}{3}\sqrt{\rho w^3}} + G_2 e^{\frac{2i}{3}\sqrt{\rho w^3}}\right] \tag{B.95}$$

Matching the linear and WKB solutions to the left and right of the turning point as before, gives:

$$G_1 = -iB_0\left(\Gamma_t + \frac{1}{2\Gamma_t}\right) \tag{B.96}$$

$$G_2 = B_0\left(\Gamma_t - \frac{1}{2\Gamma_t}\right). \tag{B.97}$$

Thus, using these formulas we can extend the WKB solution across the turning points, from the region $z \ggg 1$ to the region $z \lll 1$.

Bibliography

[1] S. Chandrasekhar, *The Mathematical Theory of Black Holes*. Oxford University Press, 1992.

[2] S. W. Hawking, *Black hole explosions?*. Nature 248 (5443): 30, 1974.

[3] J. Bekenstein, *Extraction of energy and charge from a black hole*. Phys.Rev. D7 (1973) 949953.

[4] R. Gregory and R. Laflamme, *Black strings and p-branes are unstable*. Phys. Rev. Lett. 70 (1993) 28372840.

[5] J. M. Bardeen, B. Carter, and S. W. Hawking, *The four laws of black hole mechanics*. Communications in Mathematical Physics 31 (2): 161170, 1973.

[6] S. B. Giddings and S. Thomas, *High energy colliders as black hole factories: The end of short distance physics*. Physical Review D 65 (5): 056010, 2000.

[7] S. Mathur, *The information paradox: A pedagogical introduction*. Class. Quantum Grav., Vol. 26 No. 22 (2009)

[8] S. B. Giddings, *The black hole information paradox*. Particles, Strings and Cosmology. Johns Hopkins Workshop on Current Problems in Particle Theory 19 and the PASCOS Interdisciplinary Symposium 5. arXiv:hep-th/9508151

[9] A. Almheiri, D. Marolf, J. Polchinski, and J. Sully, *Black Holes: Complementarity or Firewalls?*. JHEP 02 (2013) 062

[10] A. Almheiri, D. Marolf, J. Polchinski, D. Stanford, and J. Sully, *An Apologia for Firewalls*. JHEP 09 (2013) 018

[11] Borun D. Chowdhury and Andrea Puhm, *Decoherence and the fate of an infalling wave packet: Is Alice burning or fuzzing?*. Phys. Rev. D88, 063509 (2013)

[12] J. Maldacena, *The Large N limit of superconformal field theories and supergravity*. Advances in Theoretical and Mathematical Physics 2: 231252, 1998.

[13] S. Gubser, I. Klebanov, and A. Polyakov, *Gauge theory correlators from non-critical string theory.* Physics Letters B 428: 105114, 1998.

[14] E. Witten, *Anti-de Sitter space and holography.* Advances in Theoretical and Mathematical Physics 2: 253291, 1998.

[15] O. Aharony, S. Gubser, J. Maldacena, H. Ooguri, and Y. Oz, *Large N Field Theories, String Theory and Gravity.* Phys. Rept. 323 (34): 183386, 2000.

[16] E. Berti, V. Cardoso, and A. O. Starinets, *Quasinormal modes of black holes and black branes.* Class. Quant. Grav. 26, 163001, 2009.

[17] H. P. Nollert, *TOPICAL REVIEW: Quasinormal modes: the characteristic 'sound' of black holes and neutron stars.* Class. Quant. Grav. 16, R159, 1999.

[18] K. D. Kokkotas and B. G. Schmidt, *Quasi-Normal Modes of Stars and Black Holes.* Living Rev. Rel. 2, 2, 1999.

[19] D. Birmingham, I. Sachs, S. N. Solodukhin, *Conformal Field Theory Interpretation of Black Hole Quasi-normal Modes.* Phys. Rev. Lett. 88, 151301, 2002.

[20] F. Denef and S. Sachdev, *Quantum oscillations and black hole ringing.* Phys. Rev. D80, 126016, 2009.

[21] D. T. Son and A. O. Starinets, *Minkowski-space correlators in AdS/CFT correspondence: recipe and applications.* JHEP 09, 042 (2002)

[22] S. Kachru, A. Karch, S. Yaida, *Holographic Lattices, Dimers, and Glasses.* Phys. Rev. D81, 026007, 2010.

[23] F. Denef, *TASI lectures on complex structures.* arXiv:1104.0254 [hep-th]

[24] N. Tanahashi and T. Tanaka, *Black Holes in Braneworld Models.* Prog. Theor. Phys. Suppl.189:227–268, 2011.

[25] R. Gregory, *Braneworld Black Holes.* Lect. Notes Phys. 769:259–298, 2009.

[26] T. Kaluza, Sitzungsber. Preuss. Akad. Wiss. Berlin (Math. Phys.), 966, 1921.

[27] O. Klein, Z. Phys. 37, 895, 1926.

[28] B. Kol, *The phase transition between caged black holes and black holes.* Phys. Rep. 422, 119, 2006

[29] T. Harmark and N. A. Obers, *Phases of Kaluza-Klein Black Holes: A Brief Review.* arXiv:hep-th/0503020.

[30] S. Gubser, *AdS/CFT and gravity.* Phys. Rev. D63, 084017, 2001.

[31] M. Duff and J. Liu, *Complementarity of the Maldacena and Randall-Sundrum pictures.* Phys. Rev. Lett. 85, 2052, 2000.

[32] S. B. Giddings, E. Katz and L. Randall, *Linearized gravity in brane backgrounds.* JHEP 0003, 023, 2000.

[33] S. B. Giddings and E. Katz, *Effective theories and black hole production in warped compactifications.* J. Math. Phys. 42, 3082, 2001.

[34] N. Arkani-Hamed, M. Porrati and L. Randall, *Holography and phenomenology.* JHEP 08, 17, 2001.

[35] T. Tanaka, *Classical black hole evaporation in Randall-Sundrum infinite braneworld.* Prog. Theor. Phys. Suppl. 148, 307 (2003).

[36] R. Emparan, A. Fabbri, and N. Kaloper, *Quantum black holes as holograms in AdS braneworlds.* JHEP 0208, 043 (2002).

[37] G. Lifschytz and M. Ortiz, *Scalar Field Quantization on the 2+1 Dimensional Black Hole Background.* arXiv:gr-qc/9310008 (1993).

[38] A. L. Fitzpatrick, L. Randall, and T. Wiseman, *On the existence and dynamics of braneworld black holes.* JHEP 0611:033, 2006.

[39] P. Figueras and T. Wiseman, *Gravity and large black holes in Randall-Sundrum II braneworlds.* Phys. Rev. Lett. 107, 081101, 2011.

[40] S. Abdolrahimi, C. Cattoën, D. N. Page, S. Yaghoobpour-Tari, *Spectral Methods in General Relativity and Large Randall-Sundrum II Black Holes.* JCAP 1306, 039, 2013.

[41] R. Emparan, G. T. Horowitz, and R. C. Myers, *Exact Description of Black Holes on Branes.* JHEP 0001, 007, 2000

[42] R. Emparan, G. T. Horowitz, and R. C. Myers, *Exact Description of Black Holes on Branes II: Comparison with BTZ Black Holes and Black Strings.* JHEP 0001, 021, 2000

[43] D. Ida, *No Black-Hole Theorem in Three-Dimensional Gravity.* Phys. Rev. Lett. 85, 37583760 (2000).

[44] M. Bañados, C. Teitelboim, J. Zanelli, *The Black Hole in Three Dimensional Space Time.* Phys. Rev. Lett. 69 (1992) 1849-1851.

[45] R. Emparan, C. V. Johnson and R. C. Myers, *Surface Terms as Counterterms in the AdS/CFT Correspondence* Phys. Rev. D60, 104001, 1999.

[46] V. Cardoso and J. P. S. Lemos, *Scalar, electromagnetic and Weyl perturbations of BTZ black holes: quasi normal modes.* Phys. Rev. D63, 124015 (2001).

[47] M. Nozawa and T. Kobayashi, *Quasinormal modes of black holes localized on the Randall-Sundrum 2-brane.* arXiv:0803.3317v3 (2008).

[48] J. S. F. Chan and R. B. Mann, *Scalar Wave Falloff in Asymptotically Anti-de Sitter Backgrounds.* arXiv:gr-qc/9612026 (1996).

[49] R. A. Konoplya, *Influence of the back reaction of the Hawking radiation upon black hole quasinormal modes.* arXiv:hep-th/0406100 (2004).

[50] V. Cardoso and J. P. S. Lemos, *Quasi-normal Modes of Schwarzschild Anti-de Sitter Black Holes: Electromagnetic and Gravitational Perturbations.* arXiv:gr-qc/0105103.

[51] G. Michalogiorgakis and S. S. Pufu, *Low-lying gravitational modes in the scalar sector of the global AdS_4 black hole.* JHEP 02, 023 (2007).

[52] I. Bakas, *Energy-momentum/Cotton tensor duality for AdS4 black holes.* JHEP 01, 003 (2009).

[53] G. T. Horowitz and V. E. Hubeny, *Quasinormal Modes of AdS Black Holes and the Approach to Thermal Equilibrium.* arXiv:hep-th/9909056 (1999).

[54] S. T. Abdyrakhmanov, K. A. Bronnikov, B. E. Meierovich, *Uniqueness of RS2 type thick branes supported by a scalar field.* Grav.Cosmol. 11 (2005) 82-86

[55] A. Ahmed, L. Dulny, B. Grzadkowski, *Generalized Randall-Sundrum model with a single thick brane.* arXiv:1312.3577 [hep-th].

[56] K. Goldstein and S. Katmadas, *Almost BPS black holes.* JHEP 0905 (2009) 058

J. B. Gutowski and H. S. Reall, General supersymmetric AdS(5) black holes, JHEP 04 (2004) 048

[57] P. Galli and J. Perz, *Non-supersymmetric extremal multicenter black holes with superpotentials.* JHEP 1002 (2010) 102

[58] H. Elvang, R. Emparan, D. Mateos, and H. S. Reall, *Supersymmetric black rings and three-charge supertubes.* Phys. Rev. D71 (2005) 024033

[59] H. S. Tan and E. Teo, *Multi-black hole solutions in five-dimensions.* Phys. Rev. D 68, 044021 (2003).

[60] K. Behrndt, D. Lust, W. A. Sabra, *Stationary solutions of N=2 supergravity.* Nucl. Phys. B510, 264-288 (1998).

[61] S. D. Majumdar, *A class of exact solutions of Einsteins field equations.* Phys. Rev. 72, 390-398 (1947).

[62] A. Papapetrou, *A Static solution of the equations of the gravitational field for an arbitrary charge distribution.* Proc. Roy. Irish Acad. (Sect. A) A51, 191-204 (1947).

[63] S. D. Mathur, *Fuzzballs and the information paradox: a summary and conjectures.* arXiv:0810.4525 [hep-th].

[64] B. D. Chowdhury and A. Virmani, *Modave Lectures on Fuzzballs and Emission from the D1-D5 System.* arXiv:1001.1444 [hep-th].

[65] K. Skenderis and M. Taylor, *The fuzzball proposal for black holes.* Phys. Rept. 467, 117171, 2008.

[66] E. Andriyash, F. Denef, D. L. Jafferis, and G. W. Moore, *Wall-crossing from supersymmetric galaxies.* JHEP 1201, 115 (2012).

[67] M. Mezard, G. Parisi, and M. A. Virasoro, *Spin Glass Theory and Beyond, vol. 9.* Lecture Notes in Physics, World Scientic, 1987.

[68] A. Amir, Y. Oreg, and Y. Yospeh, *Electron Glass Dynamics.* Annual Review of Condensed Matter Physics, vol. 2, p.235-262, 2010.

[69] R. M. Wald, *General Relativity.* Chicago: The University of Chicago Press, 1984.

[70] L. Randall and R. Sundrum, *Large Mass Hierarchy from a Small Extra Dimension.* Phys. Rev. Lett. 83, 3370, 1999.

[71] L. Randall and R. Sundrum, *An Alternative to Compactification.* Phys. Rev. Lett. 83, 4690, 1999.

[72] G. W. Gibbons and S. W. Hawking, *Euclidean Quantum Gravity.* World Scientific, 1993.

[73] S. Hawking and W. Israel, *General Relativity: An Einstein Centenary Survey.* Cambridge University Press, 1980.

[74] B. Pioline and J. Troost, *Schwinger pair production in AdS_2.* JHEP 0503, 043, 2005.

[75] W. G. Unruh, *Notes on black hole evaporation.* Phys. Rev. D14, 3251, 1976.

[76] G. W. Gibbons, *Antigravitating black hole solitons with scalar hair in $N = 4$ supergravity.* Nucl. Phys. B207, 337–349, 1982.

[77] F. Denef and G. W. Moore, *Split States, Entropy Enigmas, Holes and Haloes.* JHEP 2011(11), 129, 2011.

[78] P. Galli, T. Ortin, J. Perz and C. S. Shahbazi, *Non-extremal black holes of $N = 2, d = 4$ supergravity.* JHEP 1107, 041, 2011.

[79] D. Anninos, T. Anous, J. Barandes, F. Denef and B. Gaasbeek, *Hot Halos and Galactic Glasses.* JHEP 2012(1), 3, 2012.

[80] B. D. Chowdhury and B. Vercknocki, *New instability of non-extremal black holes: spitting out super tubes.* JHEP 1202, 116, 2012.

[81] S. Ferrara, G. W. Gibbons and R. Kallosh, *Black Holes and Critical Points in Moduli Space.* Nucl. Phys. B500, 75–93, 1998.

[82] F. Denef, *Quantum Quivers and Hall/Hole Halos.* JHEP 0210, 023, 2002.

[83] M. Billo, S. Cacciatori, F. Denef, P. Fre, A. Van Proeyen and D. Zanon, *The 0-brane action in a general $d = 4$ supergravity background.* Class. Quant. Grav. 16, 2335–2358, 1999.

[84] F. Denef, *Supergravity flows and D-brane stability.* JHEP 0008, 050, 2000.

[85] D. Van Den Bleeken, *Multicenter Black Holes in String Theory.* PhD Thesis, Katholieke Universiteit Leuven, 2008.

[86] B. Bates and F. Denef, *Exact solutions for supersymmetric stationary black hole composites.* JHEP 2011(11), 127, 2011.

[87] T. T. Wu and C. N. Yang, *Dirac monopole without strings: monopole harmonics.* Nucl. Phys. B107, 365–380, 1976.

[88] Y. Kazama, C. N. Yang and A. S. Goldhaber, *Dirac monopole without strings: monpole harmonics.* Phys. Rev. D15, 2287, 1977.

[89] G. F. Torres del Castillo and L. C. Cortes-Cuautli, *Solution of the Dirac equation in the field of a magnetic monopole.* J. Math. Phys. 38(6), 2996-3006, 1997.

[90] J. A. Wheeler, *Geons.* Phys. Rev. 97, 511, 1955.

[91] D. Garfinkle and A. Strominger, *Semiclassical Wheeler womhole production.* Phys. Lett. B 256, 146, 1991.

[92] D. Brill, *Splitting of an extremal Reissner-Nordstrom throat via quantum tunneling.* Phys. Rev. D46, 1560, 1992.

[93] J. Maldacena, J. Michelson and A. Strominger, *Anti-de Sitter Fragmentation.* JHEP 9902, 011, 1999.

[94] R. Kallosh, A. Linde, T. Ortin, A. Peet and A. Van Proeyen, *Supersymmetry as a Cosmic Censor.* Phys. Rev. D46, 5278, 1992.

[95] T. Levi-Civita, R. C. Acad. Lincei (5), 26, 519, 1992.

[96] B. Bertotti, Phys. Rev. 116, 1331, 1959.

[97] I. Robinson, Bull. Akad. Polon., 7, 351, 1959.

[98] G. W. Gibbons and J. B. Hartle, *Real tunneling geometries and the large-scale topology of the universe.* Phys. Rev. D42, 2458, 1990.

[99] G. Hayward, *Gravitational action for space-times with nonsmooth boundaries.* Phys. Rev. D47, 3275, 1993.